Annals of Nuclear Energy 37 (2010) 1534–1553

Contents lists available at ScienceDirect

Annals of Nuclear Energy

journal homepage: www.elsevier.com/locate/anucene

Validation of the sodium void reactivity effect prediction using JEFF-3.1 nuclear data

J. Tommasi *, P. Archier, J.M. Ruggieri

CEA, DEN, CEA-Cadarache, DER/SPRC Bldg, 230, 13108 Saint Paul lez Durance, France

ARTICLE INFO

Article history:
Received 6 October 2009
Received in revised form 11 June 2010
Accepted 14 June 2010
Available online 10 July 2010

Keywords:
Sodium void
Validation
JEFF-3.1
ERANOS-2
TRIPOLI-4
MASURCA

ABSTRACT

Near 60 Na void experiments performed in the zero power reactors MASURCA (CEA-Cadarache) and ZPPR (Argonne West – Idaho) have been analyzed using JEFF-3.1 nuclear data and the ERANOS-2.1 (deterministic) and TRIPOLI-4 (Monte-Carlo) codes. Some comparative calculations have been performed also using either JEFF-3.1, ENDF/B-VII.0 or JENDL-3.3 nuclear data for ^{23}Na, as these three ^{23}Na evaluations show marked differences. The Na void experiments have been selected to cover spectral conditions ranging from the relatively hard flux in the outer zone of a small fast reactor to the relatively soft flux in the inner zone of a large fast reactor. For in-fuel Na void patterns, there is a good agreement between ERANOS and TRIPOLI computations, while the deterministic calculations significantly underestimate the leakage component for Na void patterns in fertile regions. The agreement between ERANOS-2.1 + JEFF-3.1 predictions and experimental values is excellent for in-fuel Na void patterns in MASURCA experiments, but a significant underestimation of the leakage component occurs for in-fuel Na void patterns in ZPPR. For fertile Na void patterns, there is a clear underestimation of the leakage component, quantitatively different for MASURCA and ZPPR experiments. Variations in ^{23}Na cross-section data also result in significant differences: ENDF/B-VII.0 and JENDL-3.3 nuclear data for ^{23}Na increase noticeably the predicted Na void worth values with respect to JEFF-3.1 data. The three ^{23}Na evaluations differ at high energy (>500 keV, and especially >2 MeV), and this stresses the need for accurate additional measurements in this energy range.

1. Introduction

The sodium void reactivity effect, or worth, is a key parameter for the design of sodium-cooled fast reactor cores (SFR), as various sodium void patterns and worth values are used to establish the feasibility and safety case of any particular design. In current large-size SFR designs with mixed U–Pu oxide fuel, large-scale voiding patterns mean high positive reactivity insertions (e.g. more than 6 $ when the fuel zone of the 1500 MWe EFR design is voided). Even if such a large-scale voiding is highly improbable, its occurrence cannot be dismissed and it must be included in the safety referential of the reactor. Safety enhancing is among the major objectives in designing advanced, "4th generation" (GEN-IV) reactors, and for SFR this is a strong incentive to minimize sodium void reactivity effects, making them as less positive as achievable or even negative, and to decrease the uncertainties on sodium void computed values, which are translated into safety margins.

Basically, removing partly or fully the sodium from a given region of a SFR induces a local hardening of the neutron spectrum, as some amount of slowing-down by sodium is removed; and an increase of neutron leakage, as the neutron mean free path is increased. The leakage increase almost always leads to a reactivity reduction. In fast reactors fueled with mixed uranium–plutonium fuel (and we shall focus here on this kind of fuels only), the spectrum hardening induces an important increase in reactivity, mainly due to an increase of $\eta = \nu\sigma_f/\sigma_a$ with energy larger for ^{239}Pu than for other fissile nuclides (Fig. 1), and also to threshold fissions in ^{238}U, ^{240}Pu,... More details on the breakdown of Na void worth using perturbation theory will be given in Section 2.

There are several ways to reduce sodium void reactivity effects, with design modifications aiming at reducing the positive spectral shift effect and/or enhancing the negative leakage increase effect (Khalil and Hill, 1991). However, when designing GEN-IV SFR with small Na void worth, an additional conflicting constraint is accounted for: the GEN-IV objective of an important breeding in the fuel itself to make a self-sustaining reactor without significant need, if any, to rely on fertile blankets. Meaning a good neutron economy (low leakage, importance of high energy neutrons associated to large η values), this is most often antagonistic to sodium void reduction. As a compromise, the GEN-IV SFR studies performed at CEA led to the following design options (Rimpault et al., 2008): large size (3600 MW thermal output), low specific power (average 230 W/cm^3 in the fuel zones instead of a typical value of ≈300 W/cm^3), increased fuel volume fraction (47% instead of values in the range 36–39%), and decreased sodium volume fraction (27% instead of values in the range 33–35%). This has been

* Corresponding author. Tel.: +33 4 42 25 75 66; fax: +33 4 42 25 70 09.
E-mail address: jean.tommasi@cea.fr (J. Tommasi).

0306-4549/$ - see front matter © 2010 Elsevier Ltd. All rights reserved.
doi:10.1016/j.anucene.2010.06.010

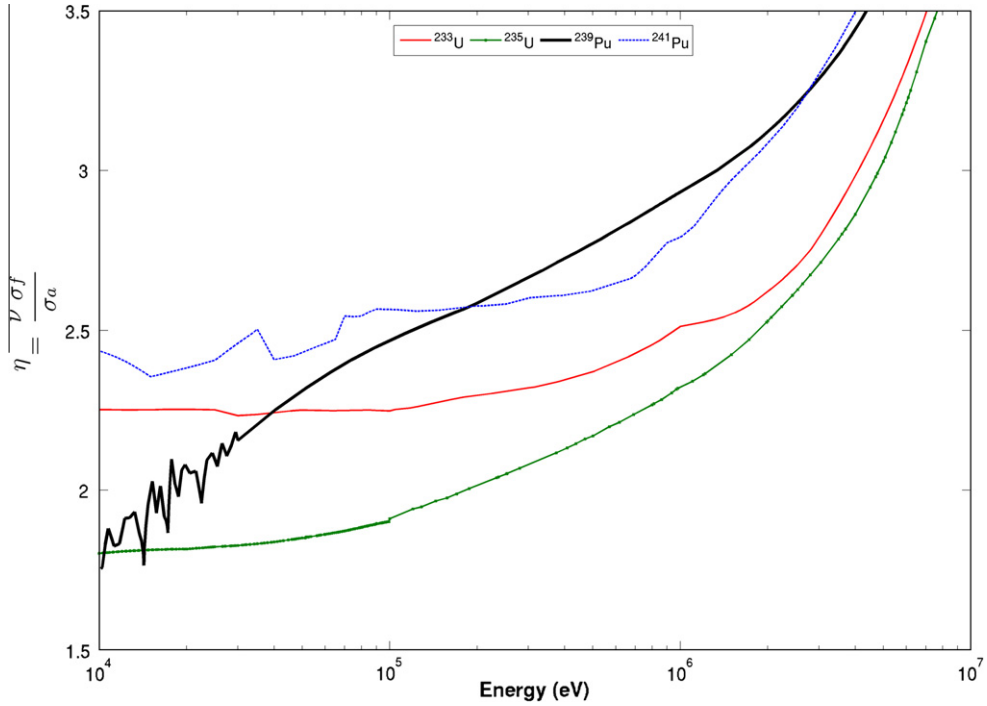

Fig. 1. $\eta = \frac{\nu\sigma_f}{\sigma_a}$ for various fissile nuclides (from the 1968-group JEFF-3.1 ERANOS library): the steeper slope for ^{239}Pu explains the high positive Na void worth values in SFR fueled with mixed U–Pu fuel, compared to SFR fueled with enriched U or mixed U–Th fuel.

done by designing large diameter fuel pins associated to small diameter spacer wires. The larger fuel volume fraction favors a high internal breeding, while the lower sodium volume fraction means a lower Na void. In turn, these larger pins and lower flow area imply a lower specific power in order to meet linear rating, heat removal and pressure drop requirements. As a result, voiding the whole fuel zone increases the reactivity by 4.9 $ (compared to 6.1 $ in the EFR design with the same thermal output), and if a sodium plenum located above the core is voided also, the Na void worth is reduced by 1 $ more. Other design options aimed at improving the safety level of the core are currently under investigation (Rimpault et al., 2008).

Such design modifications might change the sensitivity of Na void worth to nuclear data (i.e. cross-sections of ^{23}Na and other nuclides) with respect to more "classical" SFR designs, and a comparison is performed in Section 3 for simplified, academic versions of this kind of GEN-IV design and of classical SFR designs.

The accuracy of the predicted Na void worth values depends on method and nuclear data biases. Method biases can be calibrated by comparison to "benchmark" Monte-Carlo simulations, almost free of any method bias except the statistical uncertainty. Nuclear data biases can then be assessed, at least globally, by simulating integral experiments and checking the calculated values against the experimental ones. A selection of ≈60 Na void integral experiments performed on zero power reactors is presented in Sections 4 and 5 is devoted to an account of the validation work performed against experimental or benchmark simulations.

2. The physics of sodium void

As the subject in now quite classical, what follows is only a brief reminder of the breakdown of a reactivity change using perturbation theory. Consider first the multigroup diffusion theory. $\Phi_g^+(\vec{r})$ is the adjoint flux (importance) of the reference configuration, and $\Phi'_g(\vec{r})$ the forward flux of the perturbed configuration. The reactivity change from the reference to the perturbed configuration may be written as:

$$\delta\rho = \rho' - \rho = \frac{\delta k}{kk'} = \frac{\frac{P}{k} + S - A - L}{N} \quad \text{with :}$$

$$P = \int d^3r \sum_{gg'} \delta\left[\chi_g(\vec{r}) \cdot \nu\Sigma_{fg'}(\vec{r})\right] \cdot \Phi_g^+(\vec{r}) \cdot \Phi'_{g'}(\vec{r})$$

$$S = \int d^3r \sum_{gg'} \delta\Sigma_s^{g\to g'}(\vec{r}) \cdot \left[\Phi_{g'}^+(\vec{r}) - \Phi_g^+(\vec{r})\right] \cdot \Phi'_g(\vec{r})$$

$$A = \int d^3r \sum_{g} \delta\Sigma_{ag} \cdot \Phi_g^+(\vec{r}) \cdot \Phi'_g(\vec{r}) \quad L = \int d^3r \sum_{g} \delta D_g(\vec{r}) \cdot \vec{\nabla}\Phi_g^+(\vec{r}) \cdot \vec{\nabla}\Phi'_g(\vec{r})$$

$$N = \int d^3r \left[\sum_{g} \chi_g(\vec{r}) \cdot \Phi_g^+(\vec{r})\right] \cdot \left[\sum_{g'} \nu\Sigma_{fg'}(\vec{r}) \cdot \Phi'_{g'}(\vec{r})\right]$$

For sodium voiding, we have the following trends:

- production contribution P: the cross-section variation is due only to the change (increase) in self-shielding due to the sodium removal, so P is usually of small amplitude;
- scattering contribution S: the scattering cross-section variation due to sodium removal is negative, and at high energy in U–Pu fuels, the down-scattering importance change $[\Phi_{g'}^+(\vec{r}) - \Phi_g^+(\vec{r})]$ is negative, so $S > 0$;
- absorption contribution A: there is a direct term due to the removal of sodium absorption and an indirect one due to the change in self-shielding; both are usually small;
- leakage contribution L: the diffusion coefficient variation is positive when sodium is removed (as $\delta\Sigma_{\text{tr}} < 0$), and in regions where the spatial shapes of the forward and adjoint flux are similar, as this is most often the case, $L > 0$; and
- normalization integral $N > 0$: it is used to scale the result to a reactivity change.

Usually, the terms are grouped into a "central component" (CC), and a "leakage component" (LC): $\delta\rho = \text{CC} + \text{LC} = \frac{\frac{P}{k}+S-A}{N} - \frac{L}{N}$. As said

above, the main part of the central component is the spectral term S/N.

In transport theory, the transport operator $\vec{\nabla}\cdot[\Phi_g(\vec{r},\vec{\Omega})\vec{\Omega}]$ is purely geometric, without any material contribution as from the diffusion coefficient in the corresponding diffusion operator. In order to keep formally the same breakdown as above, the integrals P, S, A (and N) are computed using scalar fluxes $\Phi_g(\vec{r}) = \int_{(4\pi)}\Phi_g(\vec{r},\vec{\Omega})d^2\Omega$ and isotropic scattering cross-sections (i.e. the 0th Legendre order of the cross-section). The complement, i.e. the difference between the integrals using the angular and scalar fluxes, plus the anisotropic scattering (Legendre order > 0), replaces the L integral used in diffusion theory. The same names of central and leakage components are used.

3. Sodium void sensitivity to nuclear data

The sodium evaluated data in the recent ENDF/B-VII.0 (Chadwick et al., 2006), JENDL-3.3 (Shibata et al., 2002) and JEFF-3.1 (Koning et al., 2006) files exhibit significant differences (see e.g. Rimpault et al., 2007). The most striking discrepancies are in the high energy range and are illustrated in Figs. 2–4. For example, with respect to JEFF-3.1 sodium data:

- the ENDF/B-VII.0 total ^{23}Na cross-section is lower between 600 keV and 3 MeV, and higher between 3 MeV and 10 MeV;
- the ENDF/B-VII.0 elastic ^{23}Na cross-section is lower by ≈20% between 1 and 10 MeV; and
- the ENDF/B-VII.0 inelastic ^{23}Na cross-section is higher by more than 50% above 2 MeV.

These distinctive JEFF-3.1 elastic and inelastic cross-section values in the MeV range result from the analysis of a limited Na void experiments in zero power reactors (Fort et al., 2003). The conclusions of this analysis were used to scale the JEFF-3.1 sodium cross-sections, and this explains the markedly different behavior of the JEFF-3.1 evaluation at high energy (Figs. 2 and 3). In turn, the ENDF/B-VII.0 Na evaluation shows a marked specificity of the elastic scattering angular distribution which is more forward-peaked at high energies than for JEFF-3.1 and JENDL-3.3 (Fig. 4).

How much do such differences impact the Na void worth predictions? And what is also the influence of the cross-sections of major actinides? To answer this question we need to compute the sensitivity of Na void worth to nuclear data (cross-sections). The sensitivity of the integral parameter P to the microscopic parameter μ is defined as the ratio of the relative increase in P to the relative increase in μ causing it, i.e.: $S(P,\mu) = \frac{\mu}{P}\cdot\frac{\partial P}{\partial \mu}$. The "equivalent generalized perturbation theory" (EGPT) formalism (Gandini et al., 1986; Williams, 2007) for reactivity changes allows expressing the sensitivity of a reactivity variation $\Delta\rho = \rho_2 - \rho_1 = \frac{1}{k_1} - \frac{1}{k_2}$ as:

$$S(\Delta\rho,\mu) = \frac{1}{\Delta\rho}\cdot\left[\frac{S(k_2,\mu)}{k_2} - \frac{S(k_1,\mu)}{k_1}\right] = \frac{1}{\Delta\rho}\left[\frac{\left\langle \Phi_1^+, \left(\mathbf{A}_1 - \frac{\mathbf{F}_1}{k_1}\right)_\mu \Phi_1\right\rangle}{\langle \Phi_1^+, \mathbf{F}_1\Phi_1\rangle} - \frac{\left\langle \Phi_2^+, \left(\mathbf{A}_2 - \frac{\mathbf{F}_2}{k_2}\right)_\mu \Phi_2\right\rangle}{\langle \Phi_2^+, \mathbf{F}_2\Phi_2\rangle}\right]$$

where ρ stands for reactivity, k for multiplication factor, **F** for the production (by fission) operator, and **A** for the remaining operators in the Boltzmann equation (transport, collision, in-scattering). The index μ means the restriction of the operator to the terms involving μ (these terms are linear in μ). In order to compare the sensitivities of Na void worth values of various magnitudes, it is more convenient to compute the value $\frac{\Delta\rho}{\beta_{eff}}\cdot S(\Delta\rho,\mu)$, which can be expressed directly in ¢/% as it gives the variation in cents (with the usual convention β_{eff} = 1 $) of the Na void worth caused by a 1% variation of the microscopic parameter μ. The ERANOS-2.1 code system (Ruggieri et al., 2006; Rimpault et al., 2002), fed here by JEFF-3.1 multigroup nuclear data libraries, has extended perturbation-related capabilities, and may be used to compute the sensitivity of the multiplication factor to nuclear data (multigroup cross-sections).

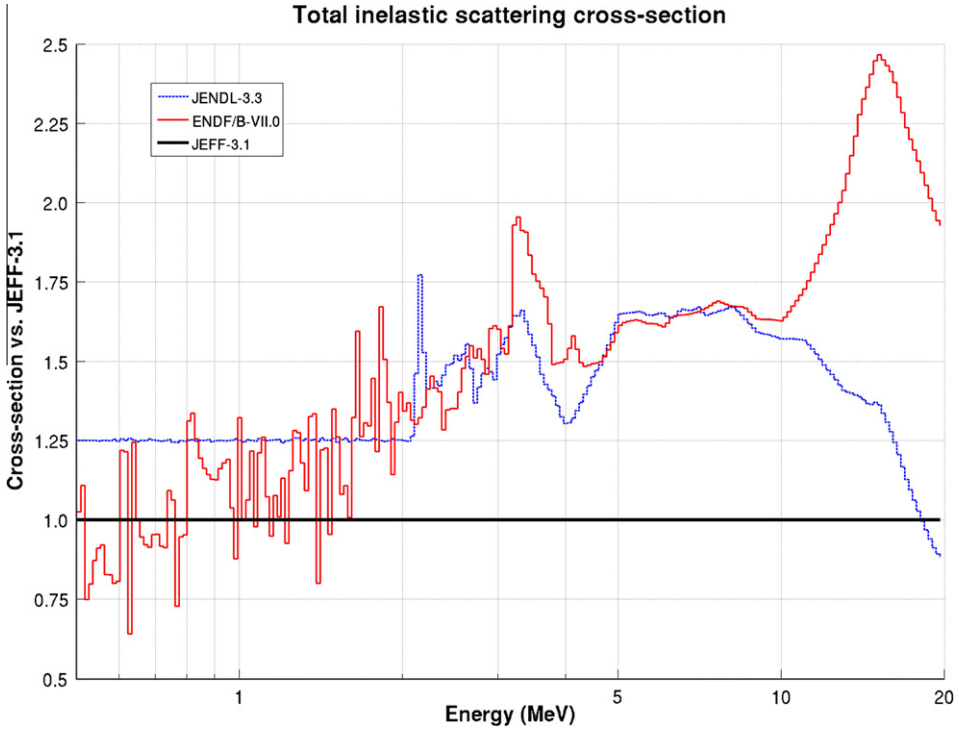

Fig. 2. ^{23}Na total inelastic cross-section: ENDF/B-VII.0 and JENDL-3.3 compared to JEFF-3.1.

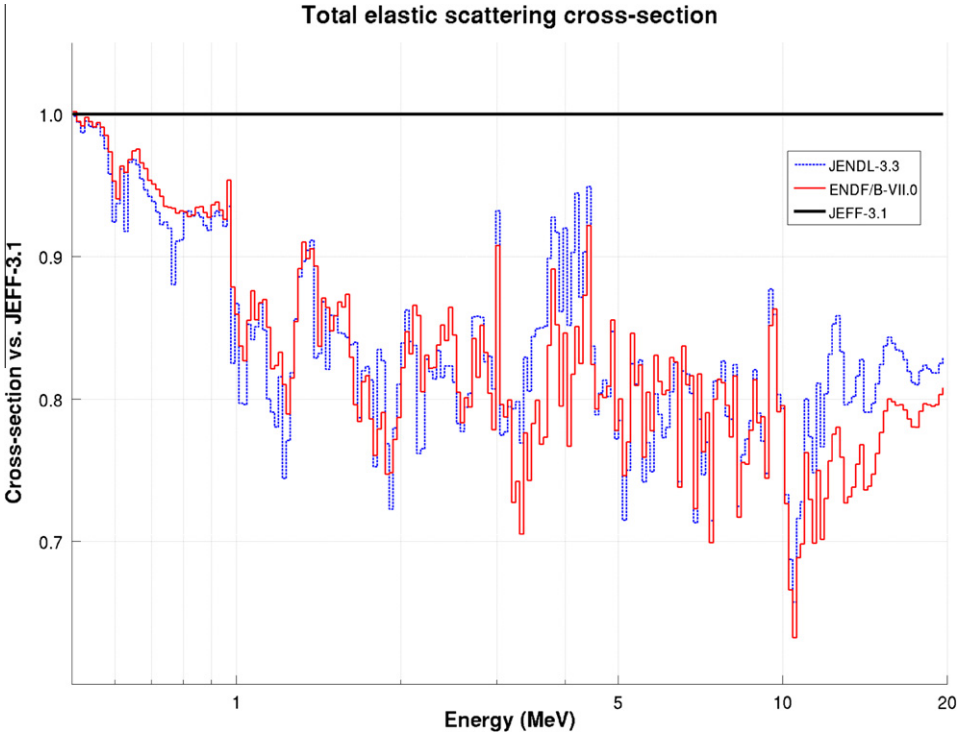

Fig. 3. ^{23}Na total elastic cross-section: ENDF/B-VII.0 and JENDL-3.3 compared to JEFF-3.1.

In order to give an idea of the sensitivity levels of Na void worth to basic nuclear data, three academic, cylindrical core models have been built and run. These are "clean" cores (no control rods) surrounded by fertile blankets, and model three different SFR designs: a small "classical" one (Phénix, abbreviated as PX), a large "classical" one (Super-Phénix, abbreviated as SPX), and a large "advanced" one resulting from the GEN-IV SFR studies at CEA (Rimpault et al., 2008). They are loaded with (U, Pu)O_2 fuel, with a plutonium isotopic composition roughly representative of the plutonium presumably available in France ca. 2035, i.e. 3.6% ^{238}Pu + 47.3% ^{239}Pu + 29.7% ^{240}Pu + 8.2% ^{241}Pu + 10.4% ^{242}Pu + 0.8% ^{241}Am. Their main characteristics are compiled in Table 1. Na void values have been computed for fresh fuel and as such are smaller than in burnt fuel conditions. When the core size increases, the magnitude of the leakage component decreases (here despite of the core flattening illustrated by the H/D ratio), while the magnitude of the non-leakage component increases from PX to SPX, and decreases from SPX to the GEN-IV SFR, due mainly in this case to the reduction in sodium volume fraction.

The most prominent sensitivity profiles computed for the three academic core models are given in Figs. 5–10, in the standard 33-group energy mesh used in ERANOS core calculations. Fig. 5 shows the Na-void sensitivities to the ^{23}Na elastic and inelastic cross-sections. The individual sensitivities, while significant, remain relatively modest (<0.5 ¢/% in absolute value for any energy group), but the uncertainties on the inelastic cross-section level are probably high (>10% on wide energy ranges). The sensitivity to the elastic cross-section is markedly different for the small-size PX core, due to a harder spectrum.

Figs. 6–9 show the Na void sensitivity profiles to the capture and fission reactions of major actinides: ^{238}U (Fig. 6), ^{239}Pu (Fig. 7), ^{240}Pu (Fig. 8), and ^{241}Pu (Fig. 9). The sensitivities to fission reactions for nuclides with fission thresholds (^{238}U and ^{240}Pu) are related to their amounts in the cores (^{238}U > ^{240}Pu), and remain modest in level, with higher sensitivity values for harder spectra (GEN-IV SFR < SPX < PX). The Na-void sensitivities to ^{238}U capture and ^{239}Pu fission may be quite high (>1.5 ¢/% in some individual energy groups), but these reactions are expected to be known within limited uncertainty (at most a few%). The Na-void sensitivities to ^{239}Pu capture, ^{240}Pu capture and ^{241}Pu fission remain lower than 0.6 ¢/% in individual energy groups, but may be associated to higher uncertainties (several%). The Na void sensitivity to the ^{16}O elastic cross-section (Fig. 10) shows a markedly different behavior for the small PX core with a harder spectrum, as for the sensitivity to the ^{23}Na elastic cross-section. As a final remark, many sensitivity profiles exhibit a marked singularity in the high-energy wing of the ^{23}Na elastic scattering resonance at 2.9 keV (energy group no. 17, 3.35–5.53 keV).

In order to translate these sensitivity profiles into uncertainty values for the computed Na void, it is necessary to assess the degree of uncertainty of the multigroup cross-section set used, through dispersion data, i.e. variances and covariances. Up to now, unfortunately, there are no dispersion data available in the JEFF-3.1 evaluated file. However, a recent international collaboration (Salvatores et al., 2008) proposed a covariance data set referred to as BOLNA[1]. Even if the values in this covariance data set are termed preliminary by their authors, and if their applicability to JEFF-3.1 cross-sections is questionable, they can nevertheless provide hints as to what may be the major contributions to Na void prediction uncertainties. Individual uncertainties are compiled in Table 2 for several reactions and macro-energy groups. The two main contributions come from the ^{23}Na inelastic cross-section between the inelastic threshold and 1.35 MeV, and from the ^{241}Pu fission between 454 eV and 2.03 keV, due to the conjunction of high computed Na void sensitivity and high reported nuclear data uncertainty. Despite high sensitivities, the contribution from ^{239}Pu fission is low, due to maybe too optimistically low uncertainties for this reaction in BOLNA (most often quoted <1%). The overall Na void uncertainty value

[1] The acronym BOLNA comes from the names of the participating laboratories: **B**rookhaven, **O**ak Ridge, **L**os Alamos, **N**RG-Petten and **A**rgonne.

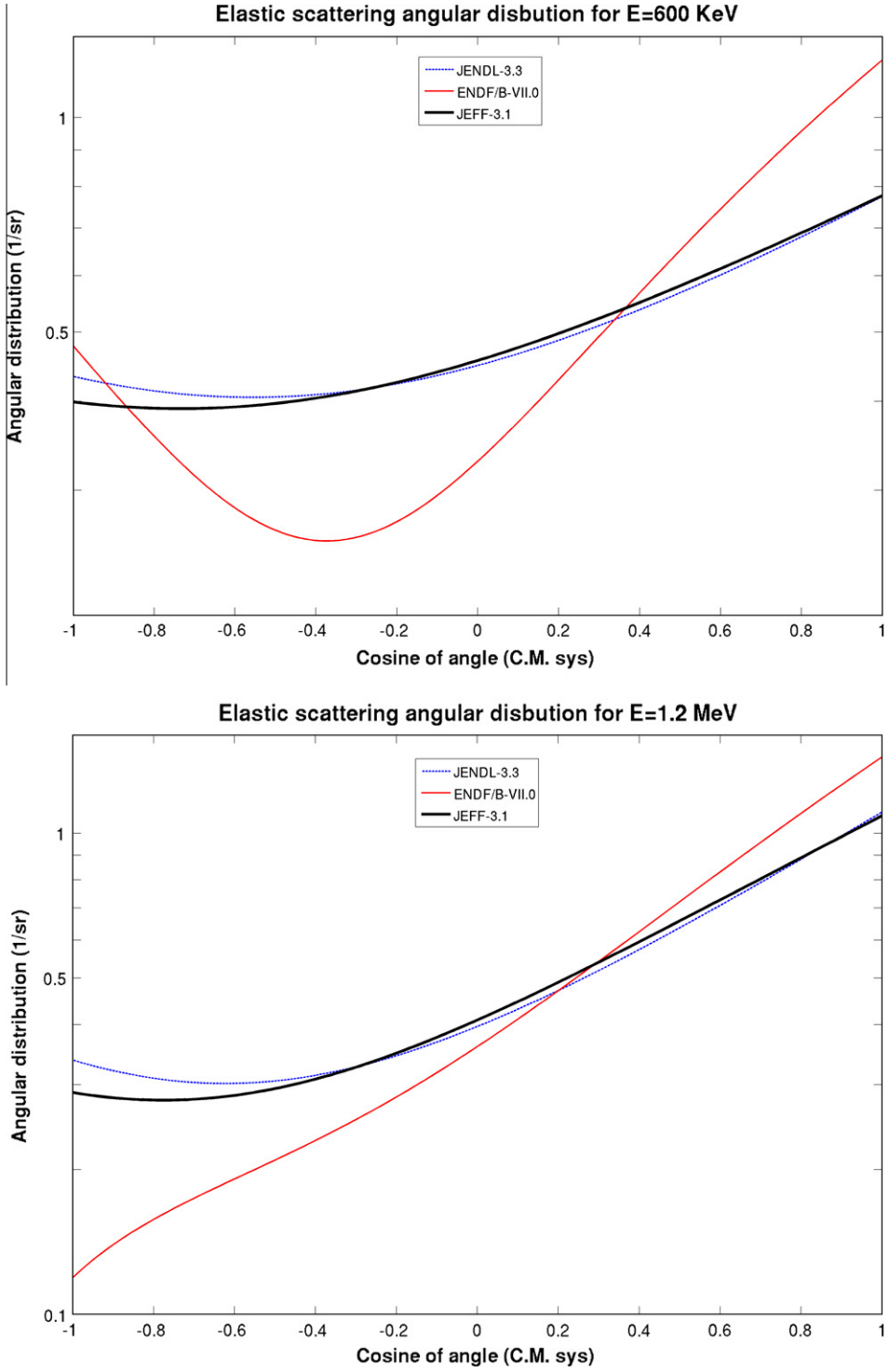

Fig. 4. JEFF-3.1, ENDF/B-VII.0 and JENDL-3.3 angular distributions for the elastic cross-sections for ^{23}Na (incident neutron energy = 600 keV and 1.2 MeV).

would result from the complex interplay of correlations; nevertheless, according to the individual values quoted in Table 2, it could be of the order of a few tens of cents (at 1 standard deviation).

4. Selection of sodium void experiments

4.1. Rationale for the selection

The Na void experiments used to check the validity of the Na void predictions must be representative of the fuel compositions and spectral conditions aimed at. To characterize quickly the spectral conditions (obviously to the cost of some loss of information), we propose to use the two following integral parameters, computed in a lattice calculation of the fuel elements: the spectrum hardness parameter r, and the importance slope parameter r^+. They are defined as follows:

$$r = \frac{1}{u_D - u_P} \qquad r^+ = \frac{\varphi_P^+}{\varphi_D^+}$$

u_P is the average lethargy at which neutrons are born by fission and u_D the average lethargy at which neutrons are removed by absorp-

Table 1
Main characteristics of the three academic designs used to compute Na void worth sensitivities to nuclear data. V = core volume (fuel zones), H = core height, D = core diameter, E_1/E_2 = Pu/(U + Pu) content in the inner/outer fuel zones. The X's are volume fractions in the fuel zones. The void reactivity worth at beginning of life of the fuel zones is also given (CC = central component, LC = leakage component, T = total).

	Phénix	Super-Phénix	GEN-IV SFR[2]
V (m^3)	1.40	11.6	18.9
H/D	0.59	0.26	0.20
E_1/E_2 (%)	21.5/28.7	16.5/20.6	14.3/16.8
X_{fuel} (%)	35.7	36.0	43.7
X_{steel} (%)	25.3	24.5	20.0
X_{sodium} (%)	36.1	33.8	27.6
$\Delta\rho_{Na}$ (\$) CC	6.28	7.63	5.83
LC	−4.18	−2.80	−1.87
T	2.10	4.84	3.95

tion or leakage; φ_P^+ is the average importance (adjoint flux) of the neutrons born by fission, and φ_D^+ the average importance of neutrons removed by absorption or leakage. The higher r, the harder the spectrum; r is correlated in particular to the plutonium content in the fuel, and then to the core size and leakage. The higher r^+, the higher the importance increase at high energy, and this is correlated to the spectral term of the Na void reactivity.

These parameters are plotted in Fig. 11 for the inner and outer fuel zones of Phénix, Super-Phénix, and two GEN-IV designs with oxide and carbide fuels (Rimpault et al., 2008). The larger the core size, the lower the spectrum hardness parameter, and the higher the importance slope parameter.

Na void patterns have been experimented in zero power reactors, and particularly in the MASURCA facility at CEA-Cadarache. The three (U, Pu)O_2-based MASURCA fuels used in past MASURCA loadings, making the ZONA series (from the acronym used for this kind of fuels in MASURCA), are also plotted on the same graph. In terms of spectrum hardness, r(ZONA3) < r(ZONA1) < r(ZONA2), and it can be seen on Fig. 11 that the ZONA fuel patterns roughly cover the spectral conditions encountered in Phénix and Super-Phénix. At MASURCA, Na void has been investigated in the past in the ZONA2 and ZONA1 fuel patterns (highlighted in green), but not in the ZONA3 pattern. It is being considered at CEA that a future MASURCA program named GENESIS, to be performed after the

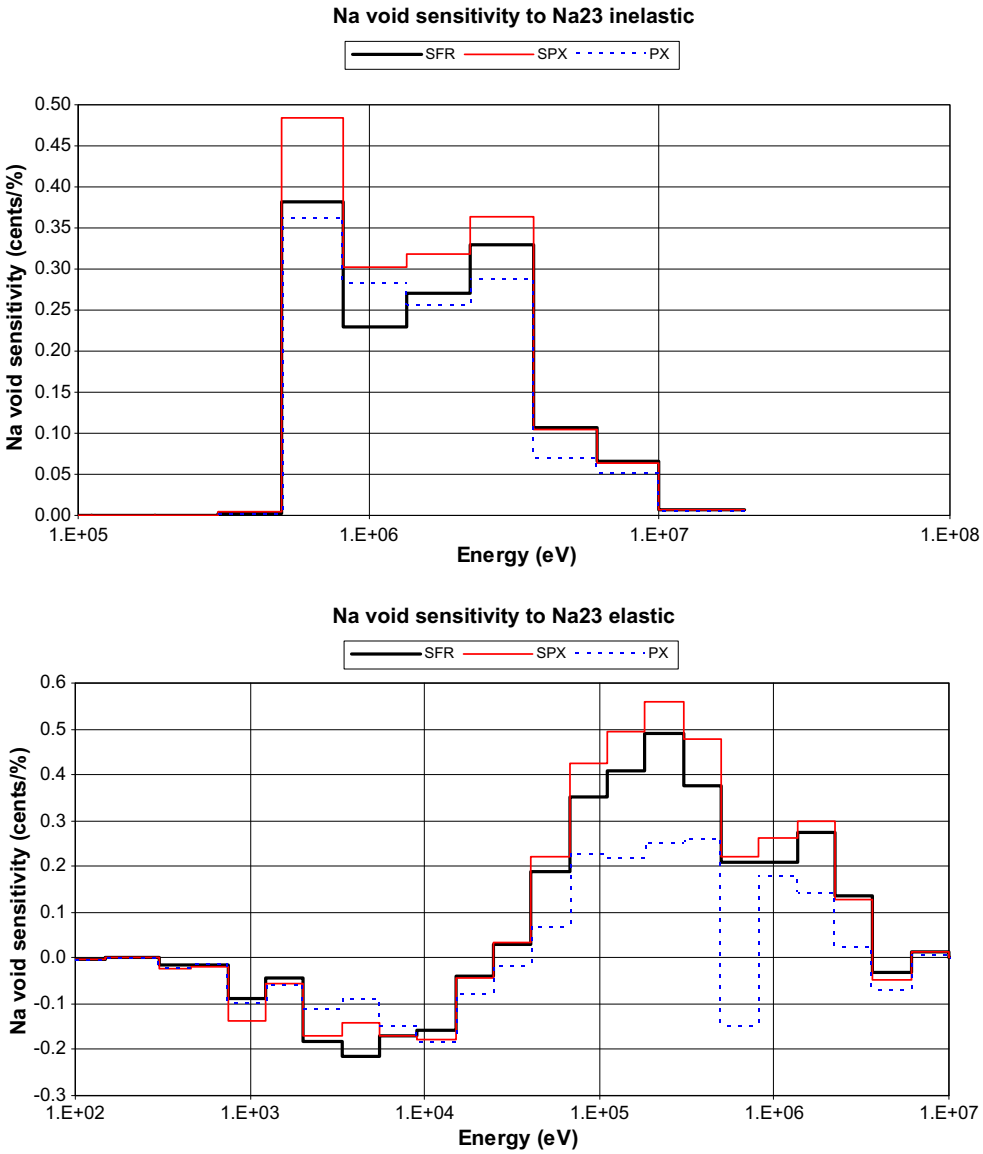

Fig. 5. 33-group Na void sensitivity to ^{23}Na cross-sections. SFR = GEN-IV SFR design[2], SPX = Super-Phénix design, PX = Phénix design.

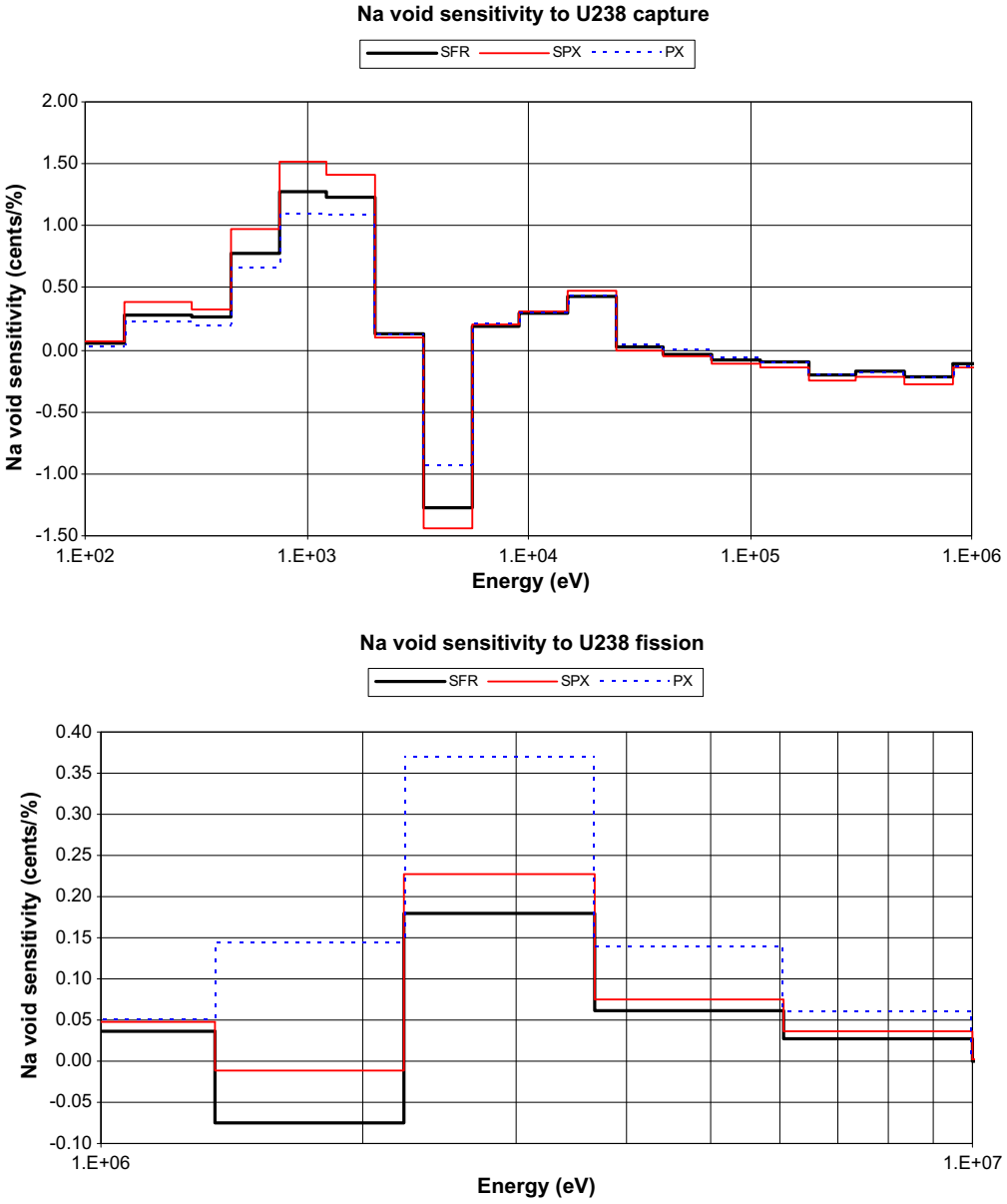

Fig. 6. 33-group Na void sensitivity to ^{238}U cross-sections.

planned refurbishment of the experimental facility (Bignan et al., 2008) will involve Na void measurements in ZONA3 fuel or even specific new ZONA patterns designed to better match the spectral conditions in a GEN-IV SFR core (such a prospective configuration is also plotted in Fig. 11, and highlighted in pink).[2]

To analyze Na void in different spectral conditions, we have selected three series of existing and documented Na void experiments:

- harder spectrum: the ZONA2A experiment in the CIRANO program (Finck et al., 1996; Rimpault et al., 1996) at MASURCA (4 Na void values);
- intermediate spectrum: the PRE-RACINE and RACINE experiments with ZONA1 fuel (Bouget et al., 1979; Humbert et al., 1984) in MASURCA (43 Na void values); and
- softer spectrum: no MASURCA experiment is now available, but a series of Na void patterns measured during the ZPPR-10A experiment performed in the frame of the JUPITER program at ANL-Idaho is available in the IRPhE database (IRPhE, 2009) (12 Na void values). This point is also represented in Fig. 11, highlighted in blue.

This set of experiments covers roughly the r and r^+ range for application SFR, from small prototypes to large commercial designs. All the cores analyzed here are surrounded by axial and radial fertile blankets. Na void in steel-reflected cores has been investigated in the CIRANO program, with ZONA2 fuel, and Na void experiments in steel-reflected cores with spectral conditions representative of GEN-IV SFR are foreseen in the future GENESIS program at MASURCA. The analysis of Na void experiments in steel-reflected cores, especially for void patterns located near the reflector, involves specific concerns about deterministic calculation methods and nuclear data of iron, and will be the subject of future work.

[2] For interpretation of color in Figs. 1–12, 14–18, the reader is referred to the web version of this article.

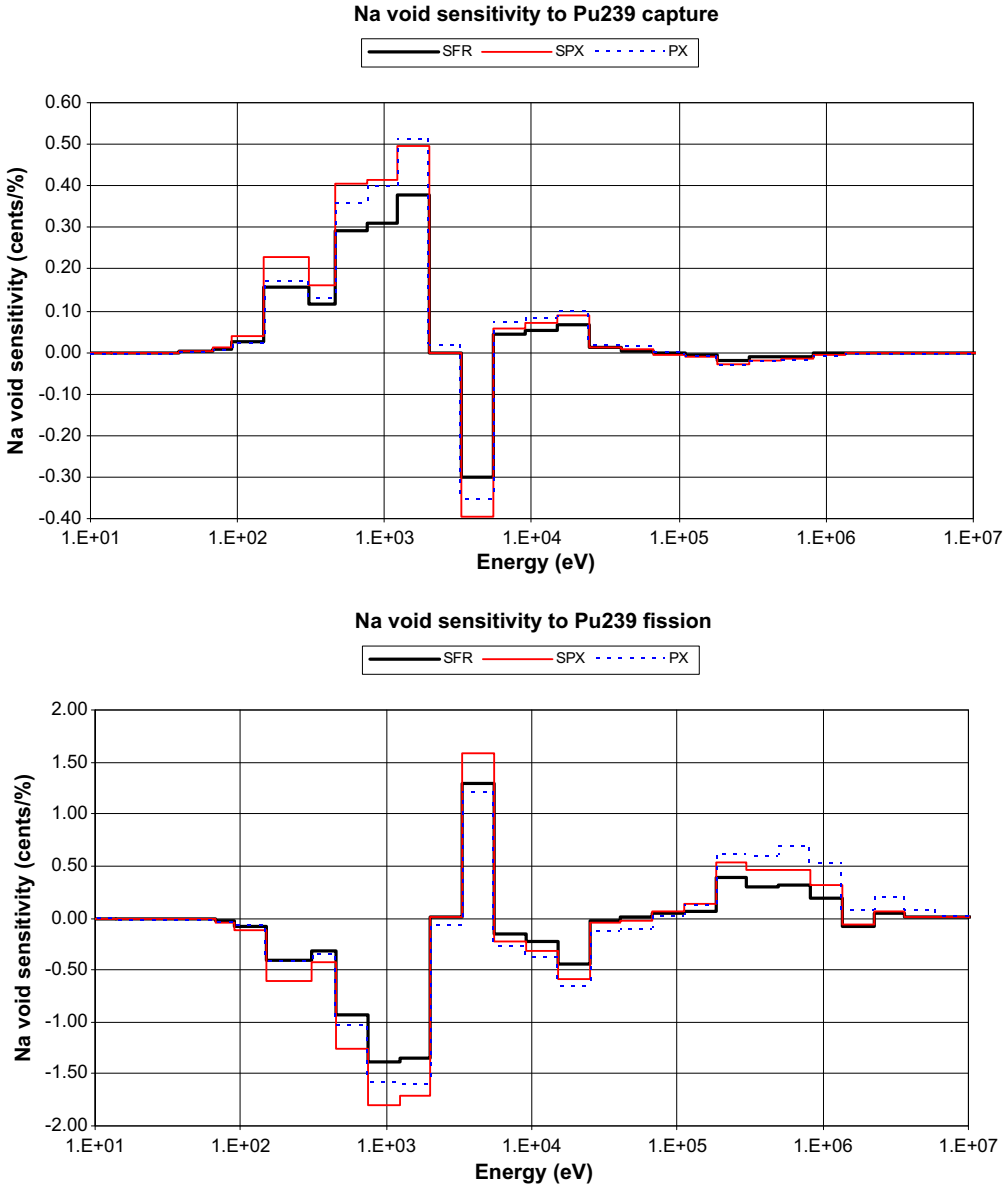

Fig. 7. 33-group Na void sensitivity to ^{239}Pu cross-sections.

4.2. Brief description of the experimental configurations

MASURCA (CEA-Cadarache, France) is an air-cooled very low power reactor (<5 kW) used for the study of fast-spectrum reactors. First achieving criticality in December of 1966, MASURCA has been used for over 40 years as a critical facility dedicated to the development of measurement techniques and the validation of various fast reactor analysis tools. Operated at near room temperature, this reactor contains sub-assemblies which consist of square wrappers loaded with square and cylindrical rods of various natures, depending on the purpose of the particular experiment and the reactor whose spectrum it is meant to emulate. The square subassembly pitch is 10.6 cm and each square wrapper has an inner dimension of 10.16 cm (4 in.) which holds an 8 × 8 rod array of 1.27 cm (1/2 in.) pitch. The loaded sub-assemblies are hung from an upper plate and the lower plate is then raised to the bottom of the assemblies connecting the air cooling path for operation. The number of rods of each type in the various ZONA fuel patterns is given in Table 3, together with the resulting fuel, steel and sodium volume fractions, and the ZONA fuel subassembly patterns are illustrated in Fig. 12.

The CIRANO ZONA2-A core (1994) is roughly cylindrical, with a fuel height of 24 in. (60.96 cm) and an equivalent fuel radius of ≈50 cm. Sodium is voided in the four central sub-assemblies, with four axial voiding patterns (Fig. 13): the central 8 in., the central 16 in., the whole 24-in. fuel height, the upper and lower 4 in. close to the axial blanket.

The objective of the PRE-RACINE (1976–1979) and RACINE (1979–1984) programs was to investigate the radial heterogeneous core concept, i.e. with fertile slabs or rings inside the fuel zone. Several cores, all with a fissile height of 36 in. (91.44 cm), and with or without fertile heterogeneities, were assembled during these programs. These cores had a quasi cylindrical structure with possibly a central fertile slab (equivalent radius ≈15 cm), a plutonium fuel zone (ZONA1 fuel, equivalent outer radius 35–45 cm), fed by an enriched uranium fuel zone (equivalent outer radius 55–65 cm), as the available plutonium fuel inventory was not enough to build a full plutonium core. Many radial Na void patterns were

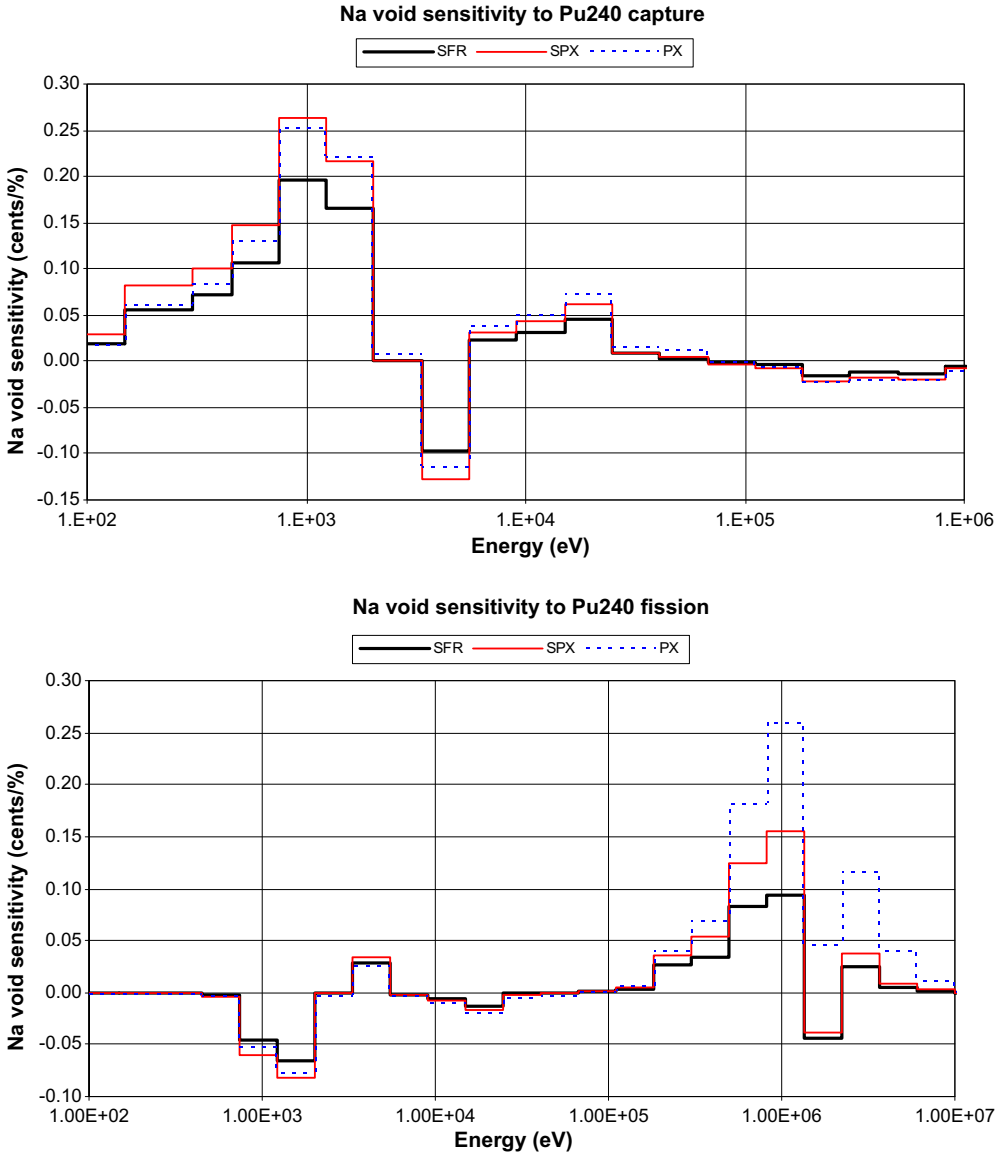

Fig. 8. 33-group Na void sensitivity to ^{240}Pu cross-sections.

investigated covering from four to more than twenty fuel tubes (see Fig. 14 and 15), and various axial voiding patterns were used also (see Fig. 16). Some large Na void values were exceeding the worth of the pilot rod (limited to 1/2 $), and they have been compensated and measured by adding or removing fuel cells at the core periphery.

The ZPPR reactor (ANL-West, Idaho) is made of two tables, one fixed and the other movable, holding horizontal drawers. The drawers are loaded with plates of various materials in appropriate patterns to emulate particular core designs. To reach criticality, the movable table is drawn close to the fixed one (<1 mm gap). The ZPPR-10A core (1978) simulates a 600 MWe SFR with two fuel zones (equivalent outer radii ≈98 cm and ≈127 cm) and 19 rod followers, surrounded by fertile axial and radial blankets. The simulated fuel height is 40 in. (101.6 cm). The Na void experiments have been performed in the inner fuel zone, and involve three radial void patterns (28, 88 and 172 fuel drawers, see Fig. 17) combined with four axial void patterns centered on the core midplane: 16 in., 32 in., 40 in. (whole fuel height), and 54 in. (fuel height + 7 in. through each axial blanket).

According to the dates of manufacture, the plutonium used in the fuel elements of MASURCA and ZPPR is of rather high grade, with the following ranges: ^{239}Pu 76–91%, ^{240}Pu 8–18%, ^{241}Pu(+^{241}Am) 0.5–4%, ^{242}Pu 0.04–0.7%. Compared to the Pu isotopic composition foreseen for the GEN-IV SFR, there is a clear deficit in higher Pu isotopes, especially ^{241}Pu and ^{242}Pu.

4.3. Experimental results

The experimental Na void values and the associated uncertainties, given as standard deviations, are split into different sets, according to different experimental conditions, such as spectrum and/or pattern voided, and are collected in several tables. Each individual Na void configuration will be referred to using an identification number (Id#), also given in the tables. Void patterns involving mainly or exclusively fuel zones are collected in Tables 4–7, and void patterns involving mainly or exclusively fertile regions (in-core slabs or rings, or axial blankets) are collected in Tables 8 and 9. Calculation results are also gathered in the same tables.

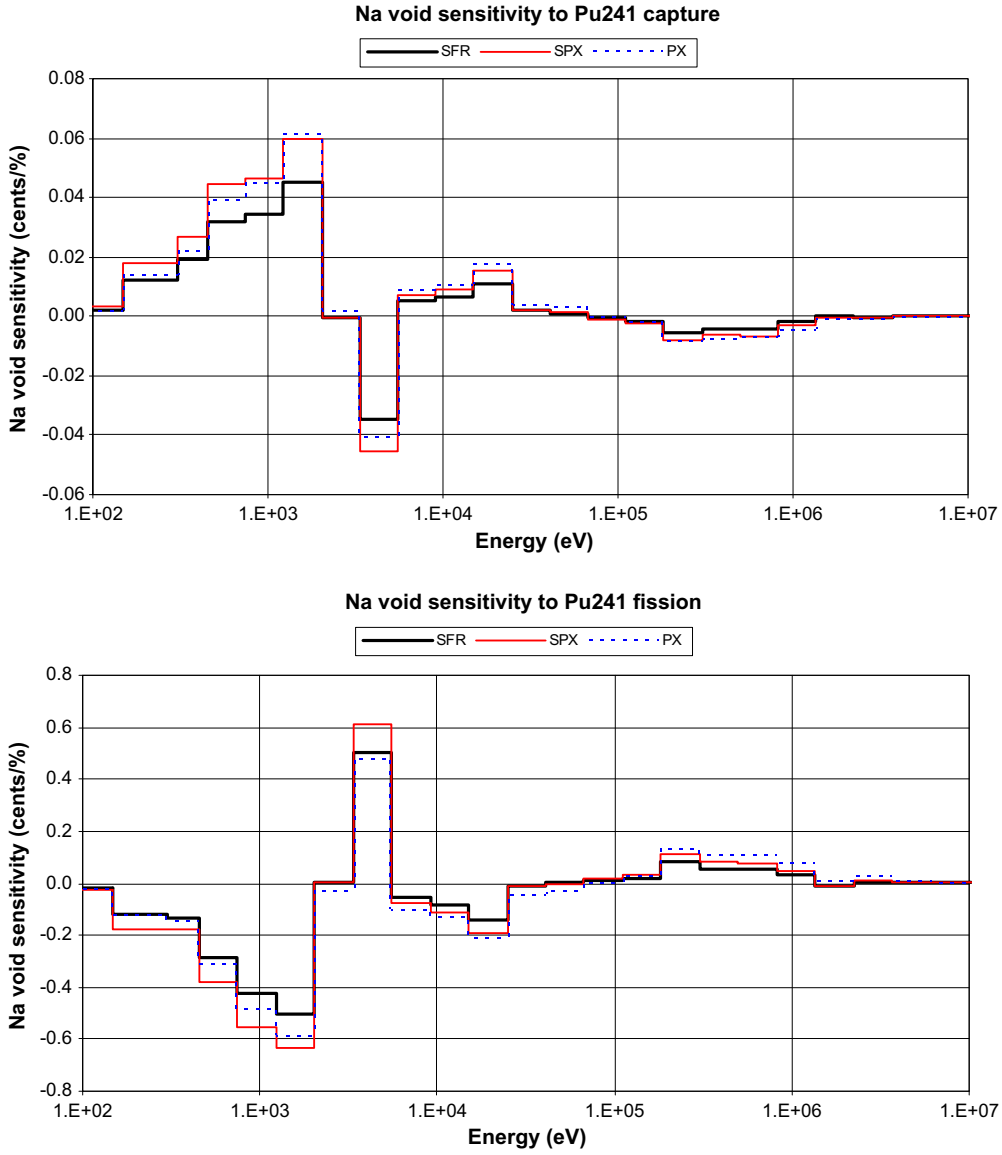

Fig. 9. 33-group Na void sensitivity to ^{241}Pu cross-sections.

Table 4 collects the 4 void patterns drawn from the CIRANO ZONA2-A experiment, Table 5 the 19 void patterns from the PRE-RACINE experiments (core + axial blanket void patterns), Table 6 the 12 void patterns from the RACINE 1A and 1D experiments and Table 7 the 9 void patterns from the ZPPR-10A experiment. Table 8 collects the 11 PRE-RACINE void patterns involving mainly or exclusively the central fertile slab and one RACINE 1A void pattern in a fertile ring, and Table 9 the 3 ZPPR-10A void patterns involving a large part of the axial blanket in addition to the core.

The CIRANO ZONA2-A, PRE-RACINE and RACINE void reactivities were recorded in pcm in the experimental reports, and the difference between the β_{eff} values computed at the time of the experimental reports and computed again now using ERANOS-2.1 + JEFF-3.1 cross-section and kinetic data was less than 2%. However, for the ZPPR-10A experiment, the discrepancy in such β_{eff} values was quite large (8%). All experimental values in pcm quoted in Tables 4–9 have been scaled to the latest β_{eff} computed value (ERANOS-2.1 + JEFF-3.1), and this explains the fractional pcm experimental values.

5. Calculations and validation

5.1. Calculation schemes

Deterministic calculations have been performed with the ERANOS-2.1 code system (Ruggieri et al., 2006; Rimpault et al., 2002). Subassembly calculations have been performed using the ECCO module of ERANOS (Rimpault, 1995), using a 1968-group energy mesh, with most individual groups covering a $\Delta u = 1/120$ range in lethargy each. The cross-cut of MASURCA sub-assemblies has been represented, either using approximate collision probabilities assessed by Roth-like methods or exact collision probabilities computed by ray tracing and numerical integration. The need for exact collision probabilities arises for Na-voided cells, which involve radial leakage channels through void rods due to the checkerboard rod loading with void rods diagonals (see Fig. 12) and axial leakage channel along the void rods. The ZPPR-10A drawer loading patterns are simplified and represented as 1-dimensional plane arrays. ECCO also condenses (in energy) and homogenizes (in space)

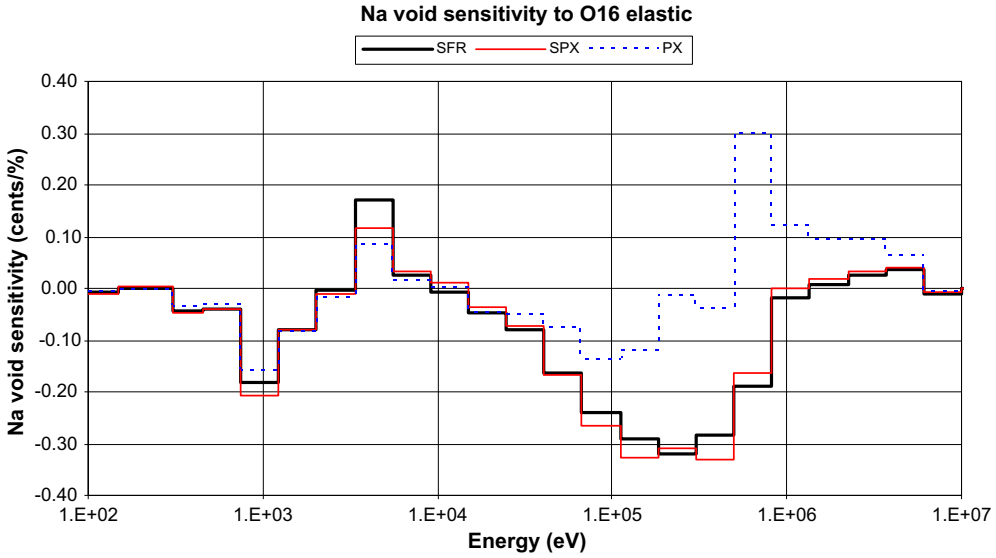

Fig. 10. 33-group Na void sensitivity to ^{16}O elastic cross-section.

Table 2
Na void sensitivities to nuclear data by reaction and energy range (GEN-IV SFR): major contributions to Na void uncertainties. S = Na void sensitivity to the reaction, ε = BOLNA uncertainty for this reaction, and $S\varepsilon$ = uncertainty on Na void due to the uncertainty on this particular reaction.

Reaction	Energy range	S (¢/%)	ε (%)	$S\varepsilon$ (¢)
^{23}Na inelastic	2.23–6.07 MeV	0.44	8.9	3.9
	1.35–2.23 MeV	0.27	12.5	3.4
	498 keV–1.35 MeV	0.61	28.0	**17.1**
^{23}Na elastic	183–498 keV	0.87	3.3	2.9
	67.4–183 keV	0.76	3.3	2.5
^{23}Na "capture"	6.07–19.6 MeV	0.05	46.4	2.4
^{238}U capture	9.12–24.8 keV	0.72	9.4	**6.8**
	2.03–9.12 keV	−0.94	3.1	2.9
^{239}Pu fission	454 eV–2.03 keV	−3.68	1.2	4.4
^{239}Pu capture	2.03–9.12 keV	−0.26	15.5	4.0
^{241}Pu fission	498 keV–1.35 MeV	0.08	16.6	1.4
	183–498 keV	0.14	13.5	1.9
	9.12–24.8 keV	−0.23	11.3	2.5
	2.03–9.12 keV	0.45	10.4	4.7
	454 eV–2.03 keV	−1.21	12.7	**15.4**

the cross-sections in order to produce equivalent homogeneous broad group cross-section sets to be used subsequently in the full core calculations (33 energy groups, most groups with $\Delta u = 1/2$). In order to use the perturbation/sensitivity capabilities of ERANOS which can be coupled only to the finite difference flux solvers available in ERANOS, the core calculations have been performed in cylindrical (RZ) geometry using the BISTRO (Palmiotti et al., 1990) finite difference Sn transport module of ERANOS. This has been shown to have a very limited impact on the predicted Na void values, with respect to full XYZ (nodal) calculations performed within ERANOS by using the VARIANT (Carrico et al., 1992; Palmiotti et al., 1993; Lewis and Palmiotti, 1997) module developed at Argonne National Laboratory. A breakdown into central and leakage components of each Na void worth is then performed. Stochastic calculations are performed also, using the TRIPOLI-4 (Both et al., 1994) Monte-Carlo code with up to 7.5×10^8 neutron histories. The sodium void reactivity is obtained by difference between two calculations (flooded and voided configuration), with a quadratic sum of their statistical uncertainties.

The nuclear data libraries used are based on JEFF-3.1 evaluated data, processed for ERANOS or TRIPOLI. The only change between the different data sets used for the calculations is for ^{23}Na cross-section data. The reference is JEFF-3.1, but some cases have also been run alternately with ENDF/B-VII.0 or JENDL-3.3 ^{23}Na data; furthermore a mixed ^{23}Na data set mixing JEFF-3.1 cross-section data and ENDF/B-VII.0 elastic scattering angular law has been used also.

5.2. Validation methodology

The objective is to perform synthetic comparisons between lists of computed and reference values related to the sodium void experiments compiled above. We assume that all uncertainties follow Gaussian laws centered on their nominal values and can be put in the form of a dispersion matrix **D** containing variances on the diagonal and covariances outside the diagonal. **D** can be put into the form $\mathbf{D} = \mathbf{SCS}$, where **S** is the diagonal matrix containing the standard deviations, and **C** the symmetric, positive definite matrix containing the correlations. Three kinds of comparison will be performed here, in order to validate calculations performed using JEFF-3.1 nuclear data:

Calculation	Validated against...
Stochastic (TRIPOLI-4.5)	Experiment
Deterministic (ERANOS-2.1)	Stochastic (TRIPOLI-4.5)
Deterministic (ERANOS-2.1)	Experiment

The comparison of stochastic calculations to experiment is performed by computing the following generalized χ^2 value, where F and E are the vectors containing the computed and experimental Na void values respectively:

$$\chi^2 = (F-E)^T \mathbf{D}^{-1} (F-E)$$

If N experimental values are involved, the reduced value χ^2/N should follow a distribution law with expected value 1 and standard deviation $\sqrt{2/N}$.

The comparison of deterministic calculations (C) to reference values (E) involves the breakdown of the deterministic results into central and leakage component: $C = \mathrm{CC} + \mathrm{LC}$, and an adjustment by two multiplicative parameters: $C \to \alpha_C \mathrm{CC} + \alpha_L \mathrm{LC}$. We define the $N \times 2$ matrix **F** by $F_{i1} = \mathrm{CC}_i$ and $F_{i2} = \mathrm{LC}_i$, the 2-vector $\alpha = \begin{pmatrix} \alpha_C \\ \alpha_L \end{pmatrix}$, and minimize the following generalized χ^2 value:

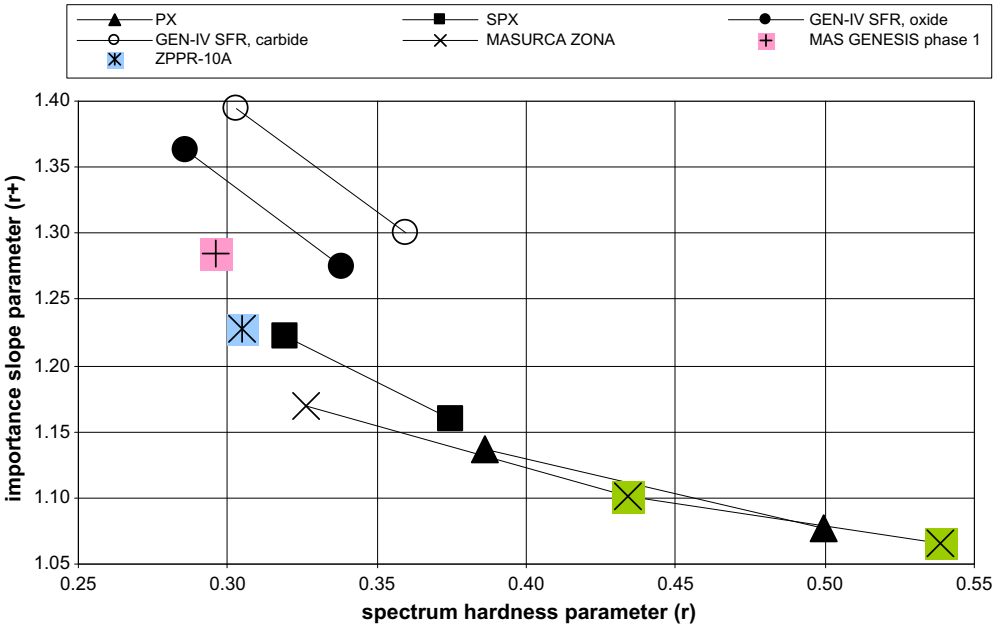

Fig. 11. (r/r^{+}) plot for various fuel types (see text).

Table 3
MASURCA fuel patterns: number of rods and volume fractions (new ZONA: reference fuel pattern for the central zone in the future GENESIS program at MASURCA).

	ZONA2	ZONA1	ZONA3	New ZONA
Number of rods				
(U, Pu)O_2	32	24	16	16
UO_2	0	8	16	32
Steel	0	0	0	0
Na	32	32	32	16
Volume fractions				
UO_2 + (U, Pu)O_2	32.4	32.3	32.3	48.4
Steel	11.3	11.2	11.2	10.9
Na	42.8	42.8	42.8	21.4

$$\chi^2 = (\mathbf{F}\alpha - E)^T \mathbf{D}^{-1} (\mathbf{F}\alpha - E)$$

This is done by putting $\frac{\partial \chi^2}{\partial \alpha} = 2(\mathbf{F}\alpha - E)^T \mathbf{D}^{-1}\mathbf{F} = 0$, yielding $\alpha = (\mathbf{F}^T\mathbf{D}^{-1}\mathbf{F})^{-1}\mathbf{F}^T\mathbf{D}^{-1}E$, and the 2×2 dispersion matrix of α_C and α_L is then $\mathbf{D}_\alpha = (\mathbf{F}^T\mathbf{D}^{-1}\mathbf{F})^{-1}$. The adjusted χ^2 is then equivalent to the sum of N Gaussian terms linked by the 2 scalar linear equations defining the optimal α_C and α_L values; hence it has $(N-2)$ degrees of freedom, and the reduced value $\chi^2/(N-2)$ follows a distribution law with expected value 1 and standard deviation $\sqrt{2/(N-2)}$. The main assumptions made are that the parameters α_C and α_L are independent from the void pattern within a given set of experimental values, and that the uncertainties on stochastic or experimental values are relevant for the analysis of the final χ^2 value (i.e. not over- nor underestimated, and given at 1σ), as well as their correlations.

The dispersion matrix **D** contains variances and covariances. Experimental Na void values are given with their standard deviations in Tables 4–9. Stochastic Na void values are obtained, within each series, by the difference between the reactivities of a reference flooded configuration (R) and a voided configuration (A); the stochastic calculations being performed independently from each other, we can assume that their variances sum up: $V(A–R) = V(A) + V(R)$. These values are also given in Tables 4–9. When comparing stochastic calculations to experiment, we have similarly $V(A - R - E) = V(A) + V(R) + V(E)$.

It is more difficult to assess the covariances to be put in **D**. Stochastic or experimental Na void values are not independent from each other, as they result from the difference between a voided configuration and a reference flooded configuration which may be the same for several Na void reactivities. Furthermore, most of the experimental Na void values are correlated because of the compensation mode of the reactivity effect (pilot rod movement, core edge cell addition or removal), temperature effects, or use of the same fuel rods.

Then, if A and B are the reactivities of two voided configurations related to the same reference flooded configuration of reactivity R, the covariance of the two Na void reactivities is:

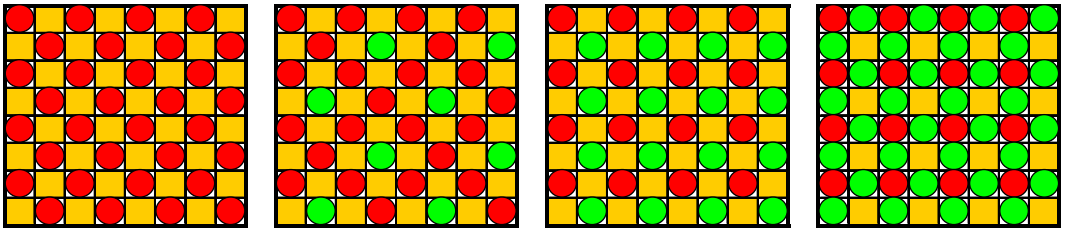

Fig. 12. ZONA fuel subassembly patterns in MASURCA. From left to right: ZONA2 = 32 (red) cyl. fuel rods + 32 square sodium (gold) rods. ZONA1 = 24 cyl. fuel rods + 8 cyl. Fertile (green) rods + 32 sodium rods. ZONA3 = 16 cyl. fuel rods + 16 cyl. fertile rods + 32 sodium rods. New ZONA (GENESIS) = 16 cyl. fuel rods + 32 cyl. fertile rods + 16 sodium rods.

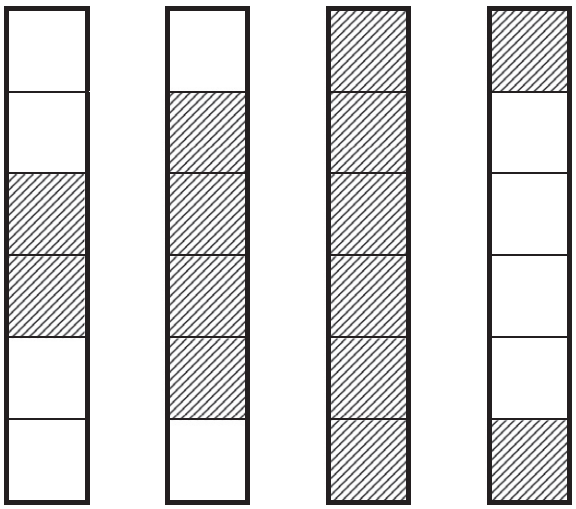

Fig. 13. CIRANO axial void patterns in MASURCA. Fuel height is 24 in. (60.96 cm), subdivided in six sections of 4 in. each. Void zones are hachured.

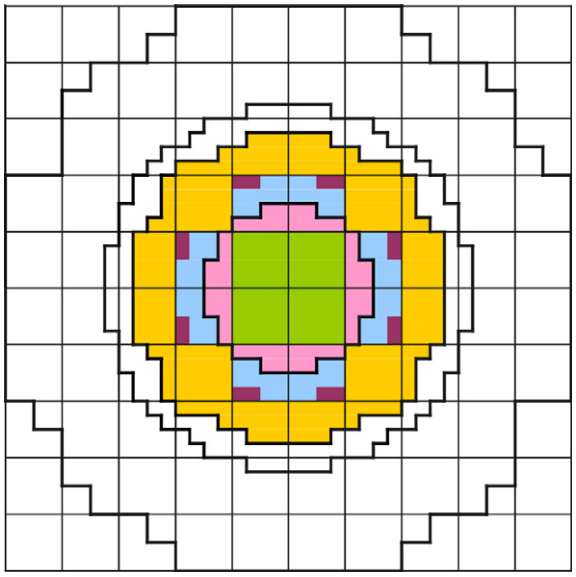

Fig. 14. PRE-RACINE radial void patterns in MASURCA each square represents a subassembly; cumulative void patterns from 4 sub-assemblies (green) to 24.25 sub-assemblies (all colors).

$$\begin{aligned}\mathrm{cov}(A-R,B-R) &= \overline{(A-R)\cdot(B-R)} - (\bar{A}-\bar{R})\cdot(\bar{B}-\bar{R}) \\ &= (\overline{A\cdot B}-\bar{A}\cdot\bar{B}) - (\overline{A\cdot R}-\bar{A}\cdot\bar{R}) - (\overline{B\cdot R}-\bar{B}\cdot\bar{R}) \\ &\quad + (\overline{R^2}-\bar{R}^2) \\ &= \mathrm{cov}(A,B) - \mathrm{cov}(A,R) - \mathrm{cov}(B,R) + V(R)\end{aligned}$$

If the reactivity measurements or computations are independent from each other, this reduces to $\mathrm{cov}(A-R,B-R)=V(R)$; and we have also $V(A-R)=V(A)+V(R)$ and $V(B-R)=V(B)+V(R)$. The value of the correlation between the two Na void reactivities can then be derived:

$$\begin{aligned}\mathrm{corr}(A-R,B-R) &= \frac{\mathrm{cov}(A-R,B-R)}{\sqrt{V(A-R)\cdot V(B-R)}} \\ &= \frac{1}{\sqrt{\left(1+\frac{V(A)}{V(R)}\right)\cdot\left(1+\frac{V(B)}{V(R)}\right)}}\end{aligned}$$

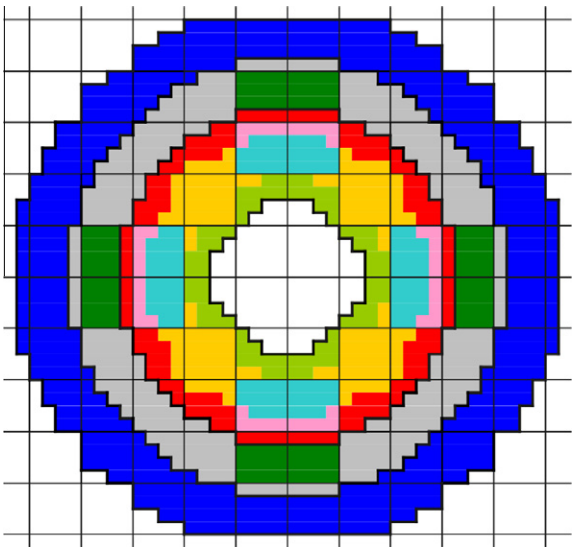

Fig. 15. RACINE radial void patterns in MASURCA. Each square represents a subassembly; cumulative void patterns.

If $A-R$ and $B-R$ result from stochastic calculations, their correlation can be computed with the above formula using the standard deviations of the individual calculations A, B, and R. However, if $A-R$ and $B-R$ are experimental values, detailed information about the individual reactivity measurements A, B, R could not be traced back generally. Hence, by lack of information we will assume that Na void reactivity measurements are not correlated to each other (i.e. correlation = 0).

Finally, when comparing stochastic calculations to experiment, we obtain in the same way as above (E and F are two experimental Na void reactivities, $\sigma(E)=\sqrt{V(E)}$ and $\sigma(F)=\sqrt{V(F)}$ are their standard deviations):

$$\begin{aligned}\mathrm{cov}(A-R-E,B-R-F) &= V(R)+\mathrm{cov}(E,F) \\ &= V(R)+\sigma(E)\cdot\sigma(F)\cdot corr(E,F) \\ \mathrm{corr}(A-R-E,B-R-F) &= \frac{\mathrm{cov}(A-R-E,B-R-F)}{\sqrt{V(A-R-E)\cdot V(B-R-E)}} \\ &= \frac{1+\frac{\sigma(E)\cdot\sigma(F)\cdot\mathrm{corr}(E,F)}{V(R)}}{\sqrt{\left(1+\frac{V(A)+V(E)}{V(R)}\right)\cdot\left(1+\frac{V(B)+V(E)}{V(R)}\right)}}\end{aligned}$$

And we assume again here that $\mathrm{corr}(E,F)=0$.

5.3. Validation of TRIPOLI-4.5 + JEFF-3.1 against experiment

There are 37 in-core void patterns computed using TRIPOLI-4.5 + JEFF-3.1. For these 37 void patterns, the reduced χ^2 is 2.09. This is clearly different from 1 with respect to the standard deviation $\sqrt{2/37}\approx 0.23$ and means that, if the statistical and experimental uncertainties are reliable, the TRIPOLI-4.5 + JEFF-3.1 results as a whole are not compatible with an exact prediction of the sodium void worth. If we look at each series individually, the Na void prediction is good for the CIRANO and RACINE experiments, overestimated for the PRE-RACINE experiments, but underestimated for the ZPPR-10A experiments.

For the 15 void patterns involving mainly fertile (in-core or blankets) computed with TRIPOLI-4.5 + JEFF-3.1, the reduced χ^2 is approximately 1.22 (associated to a standard deviation 0.37). This seems good, but Tables 8 and 9 show a roughly centered trend with the MASURCA experiments and a strong underestimation of experimental values by TRIPOLI for the ZPPR experiments.

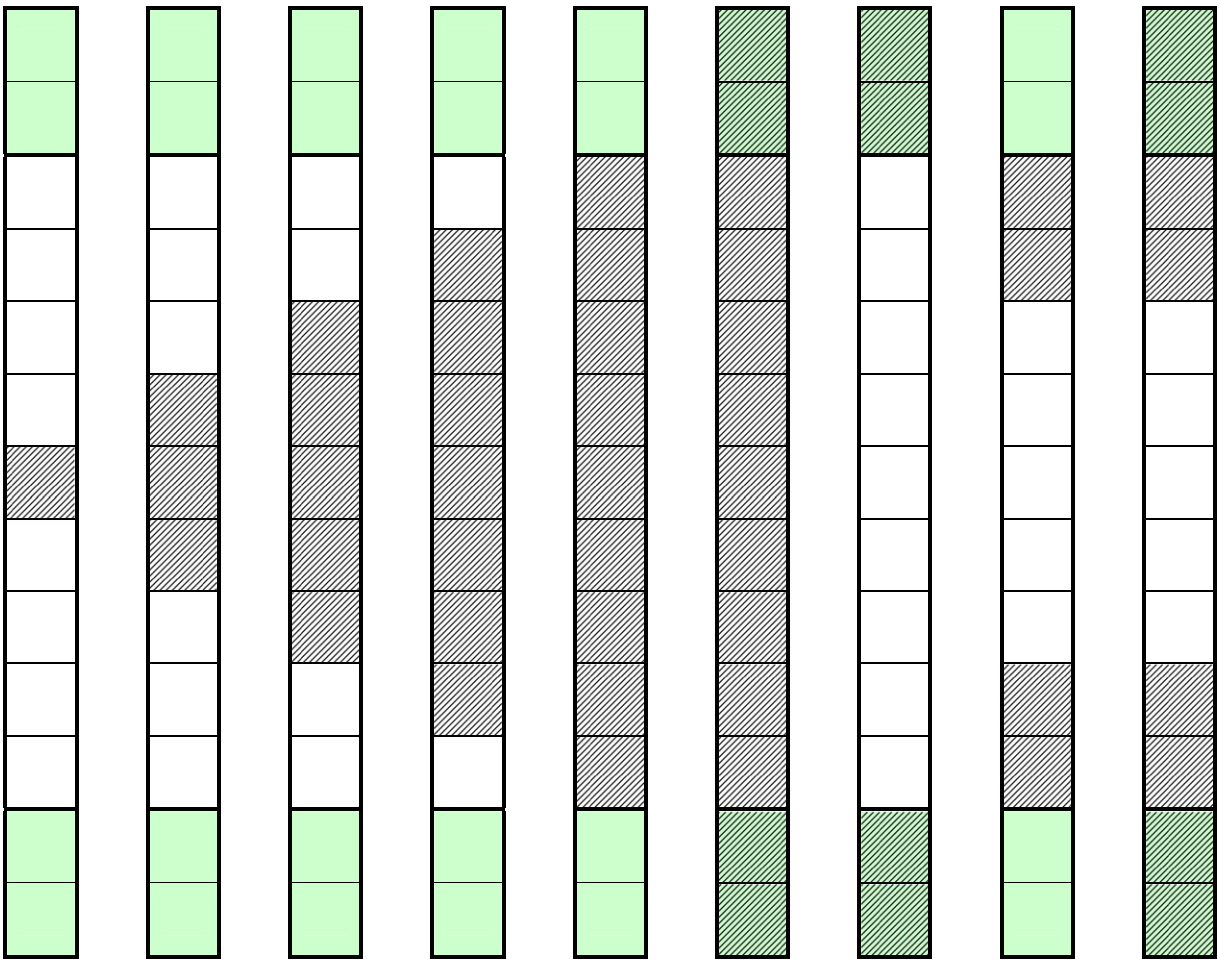

Fig. 16. PRE-RACINE and RACINE axial void patterns in MASURCA. Fuel height is 36 in. (91.44 cm), subdivided in nine sections of 4 in. each. Axial blanket 4-in. sections are represented in light green. Void zones are hachured.

This markedly different behavior of the prediction of Na void worth by TRIPOLI-4.5 + JEFF-3.1 between MASURCA and ZPPR experiments, all modeled at a very fine geometrical level (pin by pin or plate by plate), suggests either a nuclear data inadequacy sensitive to the spectral conditions or experimental biases (on compositions or reactivity worth scale). In any case, a reduced statistical uncertainty would be desirable to reach a higher discrimination level.

5.4. Validation of ERANOS-2.1 against TRIPOLI-4.5

Table 10 collects the results of the (α_C, α_L) generalized least squares adjustment for the different experimental data sets. Due to the relatively large uncertainties of the stochastic Na void computed values, the uncertainties on the adjustment parameters α_C and α_L are quite large unless a significant number of experiments is gathered. This is why all the fuel Na void reactivities have been grouped together, and this confirms the less precise trends obtained separately for the ZONA1 fuel (PRE-RACINE + RACINE) and ZPPR-10A experiments: the central component seems slightly overestimated (≈2%) by the deterministic calculation, and the leakage component is more overestimated (≈5%). The ERANOS results quoted in the table include the use of an exact collision probability routine at the lattice calculation level, and this increases by ≈4% the leakage component with respect to the approximate routine based on Roth-like methods without changing significantly the central component. It is strange that this method improvement contribute to the discrepancy observed on the leakage component (unless there are compensations with other method effects in the deterministic calculations).

The reduced χ^2 after adjustment obtained using all the 24 ZONA1 fuel Na void values is rather high (if the Monte-Carlo uncertainties are fully reliable), but it goes down to more plausible values if its three most important contributors are removed from the adjustment, without changing significantly the optimized α_C and α_L values. These three configurations (Id# 7, 12 and 16) are characterized by a large discrepancy between the TRIPOLI value and both corresponding ERANOS and experimental values, and by a discrepancy between the TRIPOLI and adjusted ERANOS values of more than 2.5 statistical uncertainties.

The consistent behavior of the adjustment observed here for the ZPPR and MASURCA Na void patterns stresses once again the markedly different behavior of both calculation tools with respect to MASURCA or ZPPR *experimental* results.

Concerning the fertile Na void values in the fertile slab or ring of the heterogeneous PRE-RACINE and RACINE cores or in a large zone of the axial blankets of ZPPR-10A, the adjustment results are compatible with a correct deterministic computation of the central component, and an underestimation of the leakage component. This is probably due to method effects at the lattice calculation level, as the fertile regions are modeled by ECCO as infinite lattice cells fed by a uniform external source issued from the fuel cell calculations, and not computed in a true multicell model, which is not fully available in ECCO. More quantitative conclusions would re-

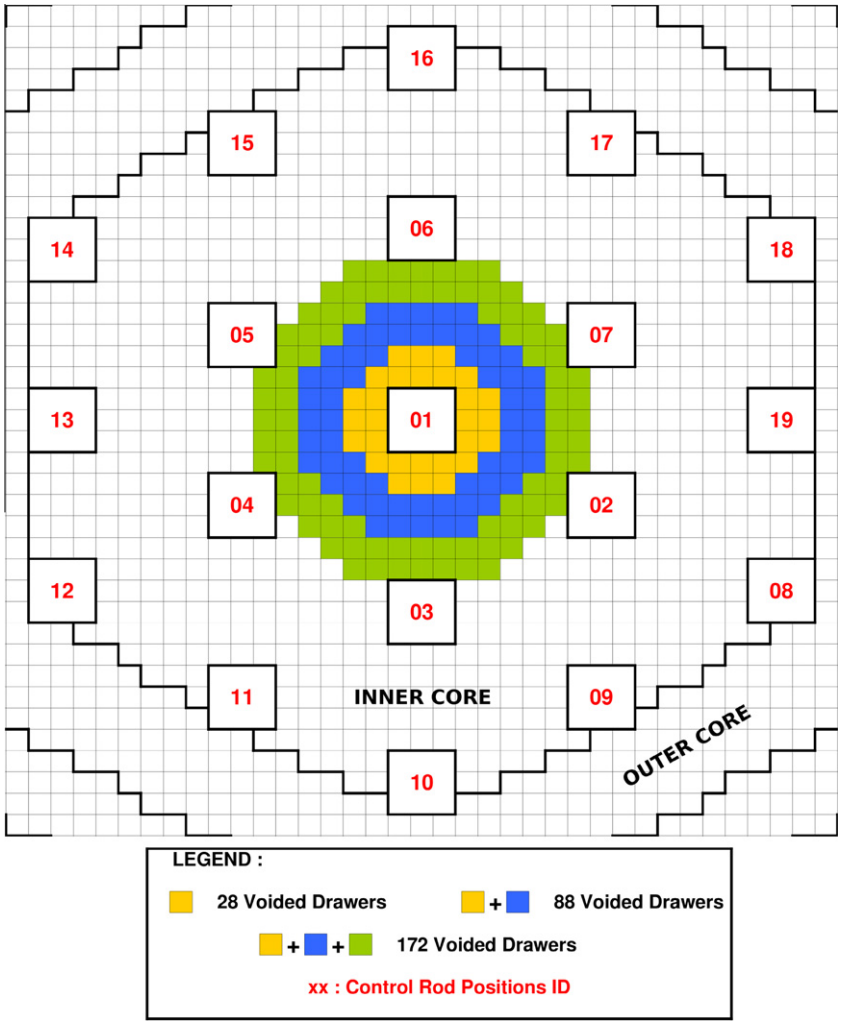

Fig. 17. Radial void patterns in ZPPR-10A.

Table 4
CIRANO ZONA2-A Na void experiments: calculated and experimental values. $V(n)$ means that n inches of fuel are voided axially. For ERANOS JEFF-3.1 the breakdown (total = central – leakage) is given.

Id#	Voided pattern	Exp. (pcm)	ERANOS JEF-2.2	ERANOS JEFF-3.1	TRIPOLI JEFF-3.1
1	$V(8)$	58.0 ± 2.7	60.8	57.8 = 70.0 – 12.2	53.2 ± 11.3
2	$V(16)$	62.5 ± 2.7	73.5	64.9 = 129.9 – 65.0	60.1 ± 11.3
3	$V(24)$	−11.0 ± 3.5	6.9	−11.2 = 172.5 – 183.7	−6.9 ± 11.3
4	$V(4+4)$	−73.8 ± 3.0	−62.8	−71.2 = 41.6 – 112.8	−85.9 ± 11.3

quire a reduction in statistical uncertainties and/or a greater number of experimental configurations involving fertile zones.

5.5. Validation of ERANOS-2.1 + JEFF-3.1 against experiment

Table 7 shows that the deterministic RZ Na void calculations are quite close to the XYZ Na void calculations, justifying the use of RZ calculations to model the void patterns and be able to use the perturbation capabilities of ERANOS. Table 11 collects the results of the (α_C, α_L) generalized least squares adjustment for the different experimental data sets. Once again, there is a clearly distinct behavior between the fits to MASURCA and ZPPR experimental Na void values. The fuel Na void patterns of MASURCA (CIRANO, PRE-RACINE and RACINE) are well predicted by ERANOS-2.1 + JEFF-3.1, as the coefficients α_C and α_L differ from each other by at most 1%, and from unity by at most 3%. The consistency between α_C and α_L is due to the use of exact collision probability routines in ECCO to account correctly for the leakage corridors in the voided fuel cells; if approximate collision probability routines were used instead, α_L would be scaled up by 3–4%, while α_C would remain almost unchanged. The optimal α_C and α_L values for the 9 ZPPR fuel void patterns are much different: according to the values quoted in Table 11, $\frac{\alpha_C^{ZPPR}}{\alpha_C^{MASURCA}} \approx 1.04 \pm 0.01$ and $\frac{\alpha_L^{ZPPR}}{\alpha_L^{MASURCA}} \approx 0.94 \pm 0.02$. A first guess would be to impute such differences to method biases, especially a bad modeling of the leakage in the voided ZPPR fuel cells, as the ZPPR fuel cells are approximated more crudely than MASURCA fuel cells with ERANOS. However, the Monte-Carlo calculations, simulating each plate within each drawer of the reactor, show the same underestimating trend that the deterministic ones, within statistical uncertainty, and consequently similar discrepancy with respect to experiment. Hence, this suggests more likely an energy-dependent bias on nuclear data (i.e. cross-section data,

Table 5
PRE-RACINE Na void experiments (fuel): calculated and experimental values. Equivalent radii of the void zones are given in cm. $V(n, p)$ means than n inches of fuel and p inches of axial blanket are voided axially.

Id#	Voided pattern	Exp. (pcm)	ERANOS JEFF-3.1	TRIPOLI JEFF-3.1
	Clean core 8% ^{240}Pu/Pu			
5	$0 < R < 11.96 - V(4, 0)$	18.4 ± 4	18.0 = 19.6 − 1.6	18.8 ± 9.6
6	$0 < R < 11.96 - V(12, 0)$	48.0 ± 3	47.2 = 57.6 − 10.4	58.9 ± 9.6
7	$0 < R < 11.96 - V(20, 0)$	55.2 ± 3	56.0 = 89.9 − 33.9	81.9 ± 9.6
8	$0 < R < 11.96 - V(28, 0)$	32.7 ± 3	36.0 = 114.6 − 78.6	47.5 ± 9.6
9	$0 < R < 11.96 - V(36, 0)$	−14.3 ± 3	−12.3 = 132.2 − 144.5	1.5 ± 9.6
10	$0 < R < 11.96 - V(36, 8 + 8)$	−53.2 ± 4	−53.7 = 150.4 − 204.1	−53.2 ± 9.6
11	$0 < R < 11.96 - V(0, 8 + 8)$	−36.8 ± 4	−36.4 = 17.5 − 53.9	−48.4 ± 9.6
12	$0 < R < 11.96 - V(8 + 8, 0)$	−66.4 ± 4	−64.8 = 41.4 − 106.2	−31.4 ± 9.6
13	$0 < R < 11.96 - V(8 + 8, 8 + 8)$	−104.3 ± 5	−105.6 = 59.3 − 164.9	−78.2 ± 9.6
14	$0 < R < 15.82 - V(36, 0)$	−30.7 ± 10	−31.7 = 225.6 − 257.3	−33.5 ± 9.6
15	$0 < R < 19.83 - V(36, 0)$	−73.6 ± 10	−71.7 = 340.2 − 411.9	−37.8 ± 9.6
	Clean core, 18% ^{240}Pu/Pu			
16	$0 < R < 11.96 - V(4, 0)$	21.0 ± 3	20.4 = 22.0 − 1.6	42.0 ± 8.8
17	$0 < R < 11.96 - V(20, 0)$	66.0 ± 3	67.5 = 100.7 − 33.2	75.4 ± 8.8
18	$0 < R < 11.96 - V(36, 0)$	0.0 ± 3	5.2 = 147.1 − 141.9	19.5 ± 8.8
19	$0 < R < 19.83 - V(36, 0)$	−20.0 ± 4	−25.5 = 378.3 − 403.8	−20.6 ± 8.8
20	$0 < R < 29.45 - V(36, 0)$	−208.0 ± 8	−225.9 = 708.5 − 934.4	−186.8 ± 5.6
	Het. core, 18% ^{240}Pu/Pu			
21	$0 < R < 29.45 - V(36, 0)$	297.4 ± 8	299.4 = 662.6 − 363.2	306.3 ± 11.3
22	$15.25 < R < 29.45 - V(36, 0)$	147.7 ± 6	149.5 = 445.9 − 296.4	162.2 ± 11.3
23	$19.83 < R < 29.45 - V(36, 0)$	89.4 ± 4	90.2 = 314.2 − 224.0	101.6 ± 11.3

Table 6
RACINE-1A Na void experiments: calculated and experimental values.

Id#	Voided pattern	Exp. (pcm)	ERANOS JEFF-3.1	TRIPOLI JEFF-3.1
	RACINE-1A			
24	$15.247 < R < 19.835 - V(20)$	27.6 ± 3	28.5 = 63.0 − 34.5	
25	$15.247 < R < 29.298 - V(20)$	119.1 ± 6	116.7 = 255.1 − 138.4	
26	$15.247 < R < 34.743 - V(12)$	238.3 ± 12	230.9 = 278.6 − 47.7	
27	$15.247 < R < 34.743 - V(20)$	186.1 ± 9	191.3 = 404.1 − 212.8	194.1 ± 7.8
28	$15.247 < R < 34.743 - V(28)$	−30.5 ± 4	−34.7 = 120.1 − 154.8	
29	$19.835 < R < 29.298 - V(20)$	84.7 ± 5	84.1 = 185.7 − 101.6	
30	$19.835 < R < 34.743 - V(20)$	154.6 ± 7	157.2 = 333.2 − 175.9	
31	$29.298 < R < 34.743 - V(20)$	60.1 ± 6	68.1 = 138.9 − 70.8	
32	$44.953 < R < 55.460 - V(20)$	168.4 ± 8	161.9 = 392.4 − 230.5	169.5 ± 7.8
	RACINE-1D Na follower			
33	$0 < R < 9.34 - V(36)$	−68.3 ± 5	−76.3 = 48.1 − 124.4	−71.6 ± 7.9
34	$9.34 < R < 32.21 - V(20)$	143.7 ± 5	149.8 = 406.0 − 256.2	154.5 ± 7.9
	RACINE-1D B_4C rod			
35	$9.34 < R < 32.21 - V(20)$	87.5 ± 5	72.9 = 258.4 − 185.5	81.1 ± 7.7

Table 7
ZPPR-10A Na void experiments: calculated and experimental values.

Id#	Voided pattern	Exp. (pcm)	ERANOS (XYZ) JEFF-3.1	ERANOS (RZ) JEFF-3.1	TRIPOLI JEFF-3.1
36	28 Drawers − $V(16, 0)$	24.0 ± 0.5	23.0	23.8 = 26.2 − 2.4	26.2 ± 7.1
37	88 Drawers − $V(16, 0)$	82.2 ± 1.0	79.9	79.4 = 86.1 − 6.7	79.7 ± 7.1
38	172 Drawers − $V(16, 0)$	157.5 ± 1.7	148.7	150.7 = 165.6 − 14.9	146.2 ± 7.1
39	28 Drawers − $V(32, 0)$	162.2 ± 1.7	154.7	155.7 = 183.2 − 27.5	146.2 ± 7.1
40	88 Drawers − $V(32, 0)$	180.0 ± 2.0	169.6	171.5 = 224.0 − 52.5	180.7 ± 7.1
41	172 Drawers − $V(32, 0)$	203.7 ± 2.3	187.5	190.3 = 277.0 − 86.7	193.2 ± 7.1
42	28 Drawers − $V(40, 0)$	199.4 ± 2.1	181.6	183.4 = 281.2 − 97.9	177.2 ± 7.1
43	88 Drawers − $V(40, 0)$	186.9 ± 2.1	168.8	170.5 = 291.7 − 121.8	169.9 ± 7.1
44	172 Drawers − $V(40, 0)$	172.6 ± 1.9	151.7	153.7 = 305.3 − 151.6	156.3 ± 7.1

not only a scale effect due to the β_{eff} value), or a bias on experimental values.

Finally, the two bottom lines of Table 11, i.e. PRE-RACINE and RACINE void patterns involving the in-core fertile zones of these heterogeneous cores, and ZPPR-10A void patterns involving fuel and a large part of the axial blankets, show that Na void worth is poorly predicted in such conditions, with also a rather large discrepancy between the optimal α_C and α_L values. This is probably due to method effects at the lattice calculation level, because the fertile regions are modeled by ECCO as infinite lattice cells fed by a uniform external source issued from the fuel cell calculations. The optimal α_C and α_L values are once more much different between MASURCA and ZPPR experimental sets.

Table 8
PRE-RACINE and RACINE-1A Na void experiments: calculated and experimental values for voided patterns including the in-core fertile slab(s). Italicized value: the void pattern extends to a limited amount of the fuel around the fertile slab.

Id#	Voided pattern	Exp. (pcm)	ERANOS JEFF-3.1	TRIPOLI JEFF-3.1
	Het. core 8% ^{240}Pu/Pu			
45	$0 < R < 15.25 - V(4, 0)$	34.7 ± 5	31.2 = 31.3 − 0.1	21.4 ± 11.3
46	$0 < R < 15.25 - V(12, 0)$	91.8 ± 7	86.6 = 89.5 − 2.9	85.1 ± 11.3
47	$0 < R < 15.25 - V(20, 0)$	126.5 ± 7	124.5 = 138.3 − 13.8	134.4 ± 11.3
48	$0 < R < 15.25 - V(36, 0)$	124.5 ± 7	131.4 = 198.2 − 66.8	127.0 ± 11.3
49	$0 < R < 15.25 - V(36, 8 + 8)$	103.1 ± 7	113.6 = 218.8 − 105.2	97.0 ± 11.3
50	$0 < R < 15.25 - V(0, 8 + 8)$	−20.4 ± 6	−14.0 = 20.5 − 34.5	−17.2 ± 11.3
51	$0 < R < 15.25 - V(8 + 8, 0)$	5.1 ± 5	10.3 = 60.5 − 50.2	3.7 ± 11.3
52	$0 < R < 15.25 - V(8 + 8, 8 + 8)$	−16.3 ± 5	−7.0 = 81.0 − 88.0	−21.7 ± 11.3
53	$0 < R < 7.33 - V(36, 0)$	33.7 ± 5	38.0 = 50.1 − 12.1	30.2 ± 11.3
	Het. core 18% ^{240}Pu/Pu			
54	$0 < R < 15.25 - V(36, 0)$	118.6 ± 4	136.3 = 202.6 − 66.3	136.9 ± 11.3
55	*$0 < R < 19.83 - V(36, 0)$*	*173.8 ± 5*	*194.7 = 329.4 − 134.7*	*189.3 ± 11.3*
	RACINE-1A			
56	$34.74 < R < 44.95 - V(20, 0)$	184.1 ± 9	214.9 = 327.8 − 112.8	188.9 ± 7.9

Table 9
ZPPR-10A Na void experiments: calculated and experimental values for voided patterns including part of the axial blankets.

Id#	Voided pattern	Exp. (pcm)	ERANOS (XYZ) JEFF-3.1	ERANOS (RZ) JEFF-3.1	TRIPOLI JEFF-3.1
57	28 Drawers − $V(40, 2 \times 7)$	165.4 ± 1.8	146.7	147.7 = 309.6 − 161.9	143.0 ± 7.1
58	88 Drawers − $V(40, 2 \times 7)$	149.7 ± 1.7	135.7	137.8 = 320.4 − 182.6	132.4 ± 7.1
59	172 Drawers − $V(40, 2 \times 7)$	130.7 ± 1.4	122.8	124.0 = 333.4 − 209.4	110.6 ± 7.1

Table 10
Result of the (α_C, α_L) least squares adjustments: validation of ERANOS-2.1 results against TRIPOLI-4 results (JEFF-3.1 library). Italicized values: the three main contributors to the reduced χ^2 after adjustment have been removed.

Experimental set	α_C	α_L	Corr.	$\chi^2/(N-2)$
Fuel Na void patterns				
ZONA2 fuel: CIRANO (4 exp. values)	1.070 ± 0.082	1.035 ± 0.075	0.707	1.56 → 1.17
ZONA1 fuel: PRE-RACINE and RACINE (24 exp. values)	0.985 ± 0.016	0.951 ± 0.014	0.934	4.50 → 2.11
Same without Id# 7,12,16 (21 exp. values)	*0.982 ± 0.016*	*0.945 ± 0.014*	*0.933*	*4.48 → 1.32*
ZPPR-10A fuel (9 exp. values)	0.973 ± 0.033	0.937 ± 0.066	0.894	1.45 → 1.32
Total in-core values (37 exp. values)	0.983 ± 0.013	0.951 ± 0.012	0.911	3.21 → 1.70
Same without Id# 7,12,16 (34 exp. values)	*0.982 ± 0.013*	*0.946 ± 0.012*	*0.910*	*3.07 → 1.20*
Fertile Na void patterns				
ZONA1: PRE-RACINE and RACINE (12 exp. values)	1.013 ± 0.036	1.172 ± 0.089	0.880	1.95 → 0.79
ZPPR-10A, fuel + ax. blanket (3 exp. values)	1.119 ± 0.123	1.249 ± 0.209	0.989	3.72 → 0.24
Total fertile values (15 exp. values)	1.001 ± 0.033	1.084 ± 0.066	0.927	1.78 → 0.96

Table 11
Result of the (α_C, α_L) least squares adjustments: validation of ERANOS-2.1 + JEFF-3.1 calculations against experiment.

Experimental set	α_C	α_L	Corr.	$\chi^2/(N-2)$
Fuel Na void patterns				
ZONA2 fuel: CIRANO (4 exp. values)	0.998 ± 0.025	1.009 ± 0.027	0.848	0.78 → 0.50
ZONA1 fuel: PRE-RACINE and RACINE (31 exp. values)	0.980 ± 0.010	0.972 ± 0.012	0.927	1.22 → 1.01
ZPPR-10A, fuel (9 exp. values)	1.025 ± 0.007	0.923 ± 0.020	0.909	44.8 → 0.48
Fertile Na void patterns				
ZONA1: PRE-RACINE and RACINE (12 exp. values)	0.974 ± 0.026	1.103 ± 0.062	0.930	5.96 → 0.83
ZPPR-10A, fuel + ax. blanket (3 exp. values)	1.236 ± 0.039	1.344 ± 0.066	0.997	168.6 → 0.29

5.6. Impact of ^{23}Na nuclear data on predicted Na void worth

The peculiar underestimation of Na void values computed with JEFF-3.1 nuclear data for ZPPR-10A has motivated the use of different cross-section sets for ^{23}Na in the nuclear data libraries used by ERANOS. The only nuclide changed in the libraries is ^{23}Na, with the following variants besides pure JEFF-3.1 data as a reference:

- JEFF-3.1 data for ^{23}Na except the angular elastic scattering law (θ_{el}), taken from ENDF/B-VII.0.
- ENDF/B-VII data for ^{23}Na.
- JENDL-3.3 data for ^{23}Na.

Table 12 displays the impact of ^{23}Na cross-section data change on core reactivity. The highest core reactivity is obtained when using pure JEFF-3.1 ^{23}Na cross-section data, with significant reductions (300–500 pcm) when shifting to pure ENDF/B-VII.0 or JENDL-3.3 ^{23}Na data. Changing only the ^{23}Na angular elastic scattering law has a very important impact in CIRANO ZONA2-A (harder spectrum), compared to a very limited one in ZPPR-10A (softer spec-

Table 12
Reactivity effects due to ^{23}Na cross-section data change.

	JEFF-3.1: *C–E*	$\Delta\rho$ (pcm) for ^{23}Na data change: JEFF-3.1 to…		
	On k_{eff} (pcm)	θ_{el} ENDF/B-VII.0	ENDF/B-VII.0	JENDL-3.3
CIRANO ZONA2A	+444	−473	−514	–
PRE-RACINE het. 8% ^{240}Pu	+501	−116	−335	−172
PRE-RACINE hom. 8% ^{240}Pu	+271	−137	−373	−192
PRE-RACINE hom. 18% ^{240}Pu	+236	−129	−365	−197
PRE-RACINE het. 18% ^{240}Pu	+328	−102	−341	−210
ZPPR-10A	+249	−16	−326	−283

trum). For CIRANO ZONA2-A, it has been checked that shifting from JEFF-3.1 to ENDF/B-VII.0 data for all nuclides, or just for ^{23}Na, brings about similar reactivity changes, suggesting almost exact compensations between the two libraries for the reactivity changes due to nuclides other than ^{23}Na.

Table 13 compiles the variations of Na void worth caused by the changes in ^{23}Na nuclear data for in-fuel void patterns, and Table 14 for void patterns including significant amounts of fertile material. As the reactivity reduction due to the use of ENDF/B-VII.0 angular scattering law is higher in hard spectra (see Table 12), it is expected that the Na void worth, being the difference between the reactivity of the voided configuration (harder flux) and the reactivity of the flooded configuration (softer spectrum) would be reduced when using ENDF/B-VII.0 angular scattering law for ^{23}Na. This is indeed what happens for in-fuel void patterns (Table 13), but not for fertile void patterns (Table 14), where method effects are important. The use of ENDF/B-VII.0 or JENDL-3.3 data for ^{23}Na results in an increase of the computed Na void worth values. This means an increase of the discrepancy between calculation and experiment for the MASURCA experiments, but a better agreement for the ZPPR-10A experiments, as shown in Fig. 18, plotting the calculation to experiment ratios (*C*/*E*) on Na void values obtained using ERANOS in XYZ core geometry (VARIANT flux solver) and various ^{23}Na cross-section data. In this particular case, with respect to the results obtained using full JEFF-3.1 data for ^{23}Na, the use of JEFF-3.1 data combined with the angular scattering law from ENDF/B-VII.0 brings a reduction of roughly 4% in the Na void prediction, but the use of full ENDF/B-VII or JENDL-3.3 data for ^{23}Na increases by 10–20% the predicted Na void value. There is also a larger shift in C/E ratios between the various experimental fuel void patterns when JEFF-3.1 ^{23}Na cross-section data is used. Note also the different behavior of the three rightmost points in Fig. 18, related to void patterns including a significant amount of the axial fertile blankets and due to method effects, as said before.

Fig. 18 and Tables 12–14 illustrate the need to confirm or invalidate the behavior of the JEFF-3.1 elastic and inelastic cross-sections of ^{23}Na above 2 MeV, a region where very few measurements are now available.

Table 13
Variations of in-fuel Na void worth due to ^{23}Na cross-section data change (ERANOS-2.1 calculations).

Id#	$\Delta\rho_{Na}$ variation (pcm) by changing JEFF-3.1 ^{23}Na to…		
	θ_{el} ENDF/B-VII.0	ENDF/B-VII.0	JENDL-3.3
5	−1.1	1.5	1.5
6	−4.2	2.8	5.7
7	−6.7	6.0	9.1
8	−4.4	11.4	11.8
9	−2.2	15.6	14.1
10	0.3	20.3	16.4
11	0.4	2.8	0.6
12	2.8	7.2	4.2
13	4.7	11.9	5.8
14	−3.0	28.3	24.3
15	−3.3	44.9	38.2
16	−0.9	1.3	2.4
17	−5.7	7.0	10.2
18	−3.4	16.1	15.3
19	−5.9	41.9	41.6
20	−4.8	89.7	80.9
21	−4.9	52.8	56.3
22	−6.7	40.5	41.4
23	−6.7	28.0	29.5
36	−1.0	1.8	2.2
37	−2.8	6.1	8.4
38	−5.4	11.8	17.6
39	−5.6	13.5	18.9
40	−6.3	17.2	24.8
41	−7.2	22.1	34.8
42	−7.0	22.9	37.8
43	−6.2	24.8	40.2
44	−4.8	27.7	46.1

Table 14
Variations of Na void worth for patterns including fertile due to ^{23}Na cross-section data change (ERANOS-2.1 calculations).

Id#	$\Delta\rho_{Na}$ variation (pcm) by changing JEFF-3.1 ^{23}Na to…		
	θ_{el} ENDF/B-VII.0	ENDF/B-VII.0	JENDL-3.3
45	−0.8	−1.7	0.4
46	0.7	1.9	4.3
47	1.3	5.7	8.2
48	1.9	10.3	10.8
49	4.9	14.2	11.8
50	1.0	3.1	1.3
51	2.1	4.9	3.0
52	1.7	7.2	4.7
53	0.0	1.2	1.6
54	2.1	11.1	10.8
55	1.7	23.1	23.7
57	−5.0	27.7	44.1
58	−4.2	28.9	77.4
59	−3.5	30.1	36.1

6. Conclusion

^{23}Na cross-section data compiled in various recent evaluated nuclear data files exhibit marked differences at energies >500 keV. Furthermore, Na void worth values are significantly sensitive not only or mainly to ^{23}Na, but also to the cross-sections of major actinides, including higher Pu isotopes. Using available dispersion data for cross-sections, this induces an uncertainty of at least a few tens of cents (at 1 standard deviation) on computed Na void values. Finally, method biases can have a significant influence on Na void deterministic computations, especially for non-fuel regions. This justifies resorting to the analysis of thoroughly performed Na void experiments in zero power reactors to establish biases between calculated and experimental values.

59 Na void experiments performed in the zero power reactors MASURCA (CEA-Cadarache) and ZPPR (Argonne West – Idaho) have been analyzed using JEFF-3.1 nuclear data and the ERANOS-2.1

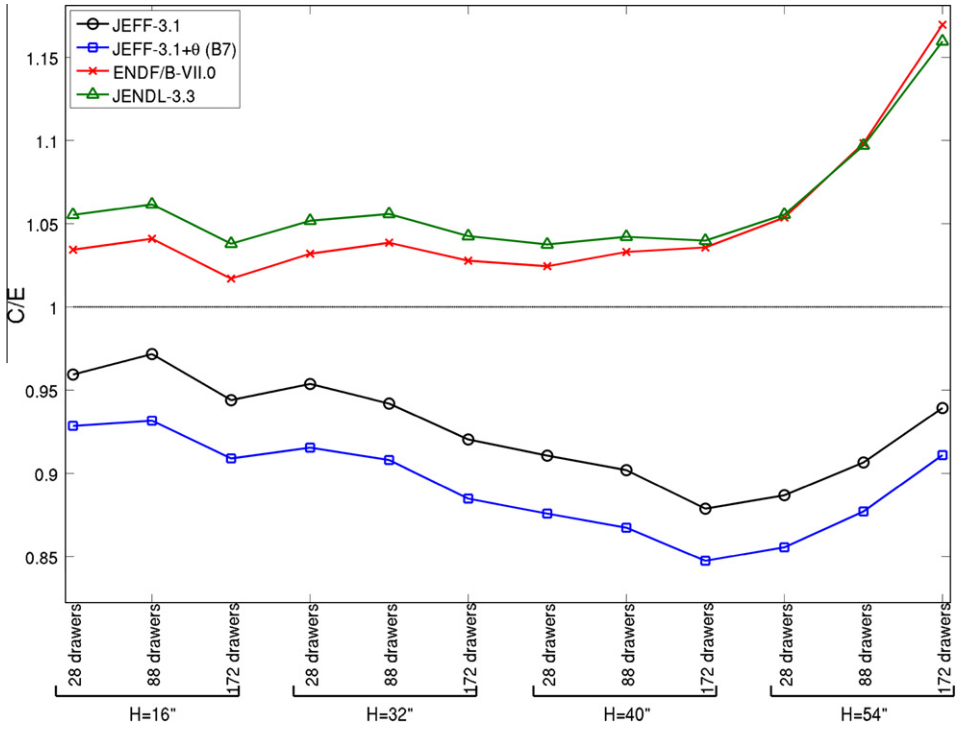

Fig. 18. ZPPR-10A void patterns: C/E obtained with various ^{23}Na data sets.

(deterministic) or TRIPOLI-4.5 (Monte-Carlo) codes. 44 Na void experiments were located in the fuel zone, and designed to cover a wide range of spectral conditions and of relative amplitudes of the central and leakage component of the Na void reactivity. The remaining 15 Na void experiments involved mainly or exclusively a fertile region (inner slab or ring, or axial blanket). Comparative calculations have been performed using JEFF-3.1 nuclear data for all nuclides except ^{23}Na, and alternatively in a few cases JEFF-3.1, ENDF/B-VII.0 or JENDL-3.3 nuclear data for ^{23}Na. The JEFF-3.1 analysis has been carried out by using a generalized least squares method to fit optimal multiplicative coefficients α_C and α_L to be applied to the central and leakage component of Na void reactivity as computed by ERANOS-2.1: $\Delta\rho_{Na} = CC + LC \rightarrow \alpha_C \cdot CC + \alpha_L \cdot LC$. Deterministic results have been checked against Monte-Carlo results and against experimental results. Stochastic results have been checked separately against experiment.

For all in-fuel void experiments, ERANOS-2.1 and TRIPOLI-4.5 results are consistent, with a slight overestimation of the leakage component by deterministic calculations ($\alpha_C \approx 0.98 \pm 0.01$ and $\alpha_L \approx 0.95 \pm 0.01$). For Na void patterns involving fertile zones, there is a trend for the deterministic calculations to significantly underestimate the leakage component, probably due to the simple models used in lattice calculations.

With respect to experimental results, the analysis underlines a clearly different behavior in the quality of Na void reactivity predictions using JEFF-3.1 data between the MASURCA experiments (rod fuel, harder and intermediate spectra) and the ZPPR experiments (plate fuel, softer spectrum). The prediction of in-fuel MASURCA Na void reactivities with ERANOS-2.1 + JEFF-3.1 is excellent ($\alpha_C \approx \alpha_L \approx 0.98 \pm 0.01$), while the prediction of ZPPR Na void reactivities is worse ($\alpha_C \approx 1.03 \pm 0.01$ and $\alpha_L \approx 0.92 \pm 0.02$). The leakage component is clearly underestimated for Na void patterns in fertile zones, with once again a different quantitative behavior between MASURCA and ZPPR experiments.

The above results might be thought to fit rather well within the 7% (1σ) target accuracy requirement reported for sodium void worth by the NEA/WPEC-26 Subgroup (Salvatores et al., 2008). However, we think that sodium nuclear data still need improvement, because of the peculiarity of the JEFF-3.1 ^{23}Na, resulting from a crude macro-group adjustment at high energy on a limited set of (MASURCA) experiments, of the scarcity of some differential data at high energy (e.g. for the inelastic reaction), and of the markedly different behavior of the comparison to experimental results from different critical facilities (MASURCA and ZPPR).

This is why ^{23}Na evaluation and validation work are currently being performed (Rochman et al., 2010; Archier et al., 2010), stressing the need to perform new differential experiments, to extend the modeling capabilities and to produce consistent dispersion data.

It is also necessary to improve the deterministic calculation models for Na void patterns outside the fuel, and to extend the integral validation database to other existing Na void measurements and to future Na void experiments in more representative conditions, as foreseen in MASURCA (the GENESIS program).

References

Archier, P., De Saint Jean, C., Noguère, G., Tommasi, J., 2010. 23 Na evaluation with CONRAD for fast reactor applications. In: Proceedings of International Conference on Nuclear Data for Science and Technology 2010 – ND 2010, Jeju Island, Korea, April 26–30, 2010 (paper no. 1298).

Bignan, G., et al., 2008. Experimental reactor physics perspectives in France. In: Proceedings of International Conference on the Physics of Reactors PHYSOR'2008, September 14–19, 2008, Interlaken, Switzerland.

Both, J.P., et al., 1994. A survey of TRIPOLI-4. In: Proceedings of International Conference on Radiation Shielding ICRS-8, Arlington, USA, 1994.

Bouget, Y.H. et al., 1979. Physics performances of a heterogeneous fast reactor core concept studied in MASURCA. Nucl. Technol. 44, 61–75.

Carrico, C.B., Lewis, E.E., Palmiotti, G., 1992. Three-dimensional variational nodal transport methods for Cartesian, triangular and hexagonal criticality calculations. Nucl. Sci. Eng. 111, 168–179.

Chadwick, M.B. et al., 2006. ENDF/B-VII.0: next generation evaluated nuclear data library for nuclear science and technology. Nucl. Data Sheets 107, 2931–3060. see at page 2964.

Finck, P.J., et al., 1996. The CIRANO experimental programme in support of advanced fast reactor physics. In: Proceedings of International Conference. on the physics of reactors PHYSOR'96, September 16–20, 1996, Mito, Ibaraki, Japan.

Fort, E. et al., 2003. Improved performances of the fast reactor calculational system ERANOS-ERALIB1 due to improved a priori nuclear data and consideration of specific additional data. Ann. Nucl. Energy 30, 1879–1898.

Gandini, A., Palmiotti, G., Salvatores, M., 1986. Equivalent generalized perturbation theory (EGPT). Ann. Nucl. Energy 13, 109–114.

Humbert, G. et al., 1984. Parametric studies on heterogeneous cores for fast breeder reactors: the pre-racine and racine experimental programs. Nucl. Sci. Eng. 87, 233–251.

IHRPhE, 2009. International Handbook of Evaluated Reactor Physics Benchmark Experiments, 2009. NEA/OECD NEA/BSC/DOC(2006)1.

Khalil, H.S., Hill, R.N., 1991. Evaluation of Liquid-Metal Reactor Design Options for Reduction of Sodium Void Worth. Nucl. Sci. Eng. 109, 221–266.

Koning, A. et al., 2006. The JEFF-3.1 Nuclear Data Library, Nuclear Energy Agency Data Bank, OECD, JEFF Report 21, NEA N°6190, 2006.

Lewis, E.E., Palmiotti, G., 1997. Simplified spherical harmonics in the variational nodal method. Nucl. Sci. Eng. 126, 48–58.

Palmiotti, G. et al., 1990. Optimized two-dimensional S_n transport (BISTRO). Nucl. Sci. Eng. 104 (1), 26–33.

Palmiotti, G., Carrico, C.B., Lewis, E.E., 1993. Variational nodal transport methods with anisotropic scattering. Nucl. Sci. Eng. 115, 233–243.

Rimpault, G., 1995. Algorithmic Features of the ECCO cell code for treating heterogeneous fast reactor assemblies. In: International Topical Meeting on Reactor Physics and Computations, Portland, Oregon, May 1–5, 1995.

Rimpault, G., et al., 1996. Experimental validation of nuclear data and methods for steel reflected plutonium burning fast reactors. In: Proceedings International Conference on the Physics of Reactors PHYSOR'96, September 16–20, 1996, Mito, Ibaraki, Japan.

Rimpault, G., et al., 2002. The ERANOS code and data system for fast reactor neutronic analyses. In: Proceedings of International Conference on the Physics of Reactors PHYSOR'2002, October 7–10, 2002, Seoul, Korea.

Rimpault, G., et al., 2007. Sodium cross-sections and covariance data for the assessment of SFR neutronic characteristics. In: Proceedings of International Workshop NEMEA-4, October 16–18, 2007, Prague, Czech Republic.

Rimpault, G., Buiron, L., Sciora, P., Varaine, F., 2008. Towards GEN-IV SFR design: promising ideas for large advanced SFR core designs. In: Proceedings of International Conference on the Physics of Reactors PHYSOR'2008, September 14–19, 2008, Interlaken, Switzerland.

Rochman, D. et al., 2010. On the evaluation of 23Na neutron-induced reactions and validation. Nucl. Inst. Methods A 612, 374–387.

Ruggieri, J.M., et al., 2006. ERANOS-2.1: the international code system for GEN-IV fast reactor analysis. In: Proceedings of International Congress on Advances in Nuclear Power Plants ICAPP'06, June 4–8, 2006, Reno, Nevada.

Salvatores, M., et al., 2008. Uncertainty and Target Accuracy Assessment for Innovative Systems Using Recent Covariance Data Evaluations, NEA/WPEC-26, NEA No. 6410, Nuclear Energy Agency, OECD, 2008.

Shibata, K. et al., 2002. Japanese evaluated nuclear data library version 3 revision-3: JENDL-3.3. J. Nucl. Sci. Technol. 39 (11), 1125–1136.

Williams, M.L., 2007. Sensitivity and uncertainty analysis for eigenvalue-difference responses. Nucl. Sci. Eng. 155, 18–36.